FABRICATION OF YBCO THIN FILMS BY PULSED LASER DEPOSITION TECHNIQUE AND THEIR CHARACTERIZATION

A Thesis Submitted to
the Graduate School of Engineering and Sciences of
İzmir Institute of Technology
in Partial Fulfillment of the Requirements for the Degree of

MASTER OF SCIENCE

in Physics

by

Şerife TOZAN

December 2010
İZMİR

We approve the thesis of **Şerife TOZAN**

_____
Prof. Dr. Doğan ABUKAY
Supervisor

_____
Prof. Dr. Bekir ÖZÇELİK
Committee Member

_____
Doç. Dr. Mustafa TEPE
Committee Member

24 December 2010

_____
Prof. Dr. Nejat BULUT
Head of the Department of Physics

_____
Prof. Dr. Durmuş Ali DEMİR
Dean of the Graduate School of
Engineering and Sciences

ACKNOWLEDGEMENTS

I first would like to thank my advisor, Prof. Doğan Abukay, for his continuous support during the master program and providing me with many opportunities and my teacher, Prof. Durmuş Ali Demir, I never forget you.

I am also thankful to Assoc. Prof. Mustafa Tepe for his support as well as his understanding in letting us use the laboratories at Ege University and Prof. Bekir Özçelik for sharing all his experience with me. I want to thank to IYTE Material Research Center staff for SEM, EDX, XRD, and AFM.

Thanks to each of my friends at Izmir Institute of Technology for providing a great atmosphere and a wonderful work place. Especially, Canan Düztürk and Handan Güneş have always been by my side and endured me. I also thank Fatma Yağız and İpek Erdoğan, who are interested in my health problem.

Finally, I am indebted to my family SERKAN and SAADET TOZAN for their support in all the choices I have made. I am forever grateful to my husband, TAYFUN RÜZGAR, for his love and encouragement.

ABSTRACT

FABRICATION OF YBCO THIN FILMS BY PULSED LASER DEPOSITION TECHNIQUE AND THEIR CHARACTERIZATION

This thesis focuses on pulsed laser deposition (PLD) system, fabrication of high temperature superconducting YBCO thin films and their characterization. In this study, the electrical and structural studies performed on laser deposited YBCO films have shown that films produced by PLD. The thin films were characterized in detail by employing structural XRD, SEM, EDX and AFM and electrical (R-T) measurements.

During this work, pulsed laser deposition system used to grow superconducting thin film on MgO single crystal substrate. Firstly PLD system was carried out by using different growth parameters. Deposited films was cooled down in situ under an oxygen atmosphere at a given pressure. The deposition tecnique has emerged as a very powerful method to make composition and microstructure controlled superconducting YBCO films.Thanks to rapid heating and evaporation of the target and interaction of the laser beam with evaporated materials leading to formation of a high temperature plasma PLD system is different from other thin film growth system.However, major problem was particulates emmission which was shown SEM,we solved this problem by chaning distance between target and substrate, and laser power. Furthermore Electron Dispersive X-Ray Spectroscopy (EDX) method was used to identify the chemical contents of the films.The relation between critical temperature and oxygen deficieny was investigated by means of electrical resistance R(T) and x-ray diffraction measurements.Finally, our results were compared to literature and explanied similarites.

ÖZET

YBCO İNCE FİLMLERİNİN PULS-LAZER YIĞMA TEKNİĞİYLE YAPILMASI ve KARAKTERİZASYONU

Bu çalışmanın temel amacı YBCO ince filmlerinin puls-lazer yığma (PLD) tekniğiyle üretilmesi ve yapısal özelliklerinin incelenmesidir. Bu çalışmada lazer yığmasıyla elde edilen filmlerin elektiksel yapısal özellikleri çalışılarak PLD sistemiyle YBCO süperiletken filmler üretilmştir. İnce filmlerin yapısal XRD, SEM, EDX ve AFM, elektriksel özellikleri de RT ve manyetik alınganlık ölçümleri kullanılarak detaylı olarak karakterize edilmiştir.Bu çalışma sırasında MgO alt taşlar üzerine epitaxial olarak büyütüldü.Öncelikle YBCO ince filmler, PLD sisteminde farklı büyütme parametreleri kullanılarak yapıldı. Epitaxial olarak büyüyen filmler belirli bir basınçta belli bir sıcaklıkta soğumaya bırakıldı.

PLD film büyütme tekniği kontrollu bir biçimde farklı bileşikte ve microyapıda YBCO süperiletken ince film üretmek için güçlü bir methottur. PLD sistemi, hedef malzeme yüksek sıcaklıkta lazer demetiyle gaz fazında buharlaştırılmasından dolayı diğer film büyütme sistemlerinden farklıdır. Ancak SEM görüntülerinde görüldüğü gibi çok fazla parçacık yayılması vardır. Lazerin gücünü ve hadefle malzeme arasındaki mesayi değiştirerek bu sorunu çözdük. Ayrıca, Enerji Dağılımlı X-ışını Spektoskopisi yöntemi filmin kimyasal içeriğini bulmak için kullanılmıştır.Kritik sıcaklıkla oksije eksiklliği arasındki ilişli R(T) ve X-ışını kırınımı (XRD) ölçümleriyle incelenmiştir. Sonuç olarak, bulduğumuz sonuçlar literaturle karşılaştırarak açıklandı.

To my Lovely Family

TABLE OF CONTENTS

LIST OF FIGURES

LIST OF TABLES

CHAPTER 1

INTRODUCTION

Superconductivity was discovered in 1911 by Heike Kamerling Onnes, who was studying the resistance of solid mercury .When he cooled it to the temperature of liquid Helium, 4 degrees Kelvin, its resistance suddenly vanished. Onnes showed that many metals like Pb, Hg, Sn and Al undergo a phase transition at some temperature T_c, to a state having a zero resistance. The next step in understanding superconductivity is the exclusion of magnetic flux in a superconductor, discovered by Meissner and Oschsenfeld in 1933 (Onnes, 1911).

The properties of superconductors were unusual that it took decades to explore many phenomena related with it. A satisfactory microscopic theory of superconductivity was developed by Bardeen, L. Cooper and J. Schrieffer. They developed BCS theory to explain the physical mechanism of superconductivity. This theory earned them the Nobel Prize in 1972. According to the BCS theory, the attractive interaction between electron and electon lead to directly by the interaction between the electrons and the vibration crystal lattice in superconductor. This is known the electron-phonon interaction. An electron in the lattice which moves through a conductor will attract nearby positive charges. This deformation of the lattice is brought about another electron with opposite spin to move into the region of higher positive charge density. This increase in positive charge will attract another electron. The two electrons are held together, called a Cooper Pair. Cooper pair which have opposite momentum and spin. Nevertheless, in the superconducting state and in the absence of current flow a cooper pair is a system with zero momentum and zero spin like a boson. Lattice imperfections and vibration have no effect on cooper pairs. The total momentum the pair is zero so that it moves without scattering in the lattice which leads to zero resistance (Barden, 1957).

In 1970s many elements and compounds were found to be superconducting with higher superconducting transition temperatures. In 1986, Johannes George Bednorz and Karl Alexander Müller discovered the first high temperature superconducting materials out of metallic systems, namely $La_{5-x}Ba_xCu_5O_{5(3-x)}$,

which consist of barium, lanthanum, copper and oxygen, which had a transition temperature of 35 K (Nobel Prize in Physics, 1987) (Bednorz, 1986). It was shortly found by M.K Wu that replacing the lanthanum with yttrium, making $YBa_2Cu_3O_7$ (YBCO), raised the critical temperature to 92 K, which was economically important because the cheap and easily available liquid nitrogen could be used as a refrigerant (at atmospheric pressure, the boiling point of nitrogen 77 K) (Wu, 1987). Following the discovery of the high T_c superconductivity, BSSCO ($T_c = 11OK$) (Maeda, 1988), TBCCO ($T_c = 125K$) (Parkin, 1988) and $Ba_2Ca_2Cu_3O_{1+\times}$ ($T_c = 130K$)

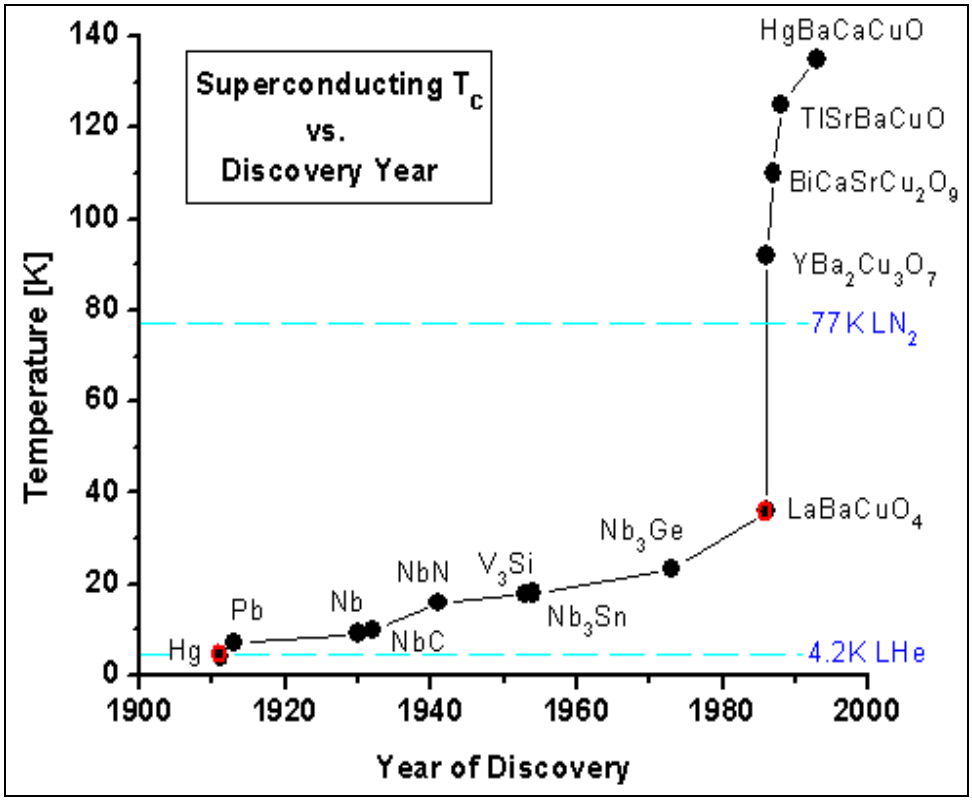

Figure 1.1. Discovery of materials with successively higher T_c ' s over the last century (it refers to a Nobel Prize for their discovers)

Since the discovery of he high T_c superconductor, many works have concentrated on these new materials. One of the most important topics is the thin film deposition because thin film growth is the basic technique for future electronic application. However, epitaxial growth of high-T_c compounds in thin film form was found to be challenging because the high-T_c materials have characteristic properties which require growth conditions and growth techniques different from those used to deposit films of classical superconductors like Nb or for films of semi-conductors like

Si or GaAs. Some of the difficulties associated with the fabrication of high-T_c thin films the realization of correct elemental stoichiometry, proper oxygen content and optimum crystallographic alignment in the films. A lot of progress have been made during the current decades in solving the problems associated with the epitaxial growth of high-T_c materials and now excellent films are being made, notably by laser ablation, PLD.

The first report of a high-T, superconducting thin films about PLD, although with reduced T_c was published by Somekh in 1987 within three months, Enomoto (1987) were successful in obtaining films with high-T_c and critical current density (I_c). Since then, thin films of HTSC have been reported by a large number of group worldwide (Neifelt, 1988). Some techniques of growth require high temperature annealing after growth (ex-situ) while some techniques grow a film in correct crystal structure (in-situ). In preparing films by ex-situ annealing the metallic elements are deposited in approximately the correct composition as an amorphous layer, usually in compound form with oxygen and possibly fluorine. If they are deposited on suitable substrates, subsequent annealing in air or oxygen at high temperature results in thin film to crystallize by a solid state regrowth mechanism to form a polycrystalline layer (Naito, 1987). Depending on the substrate, the films may be textured with one orientation aligned in a particular direction or epitaxial with the same crystal orientation as the underlying substrates. Since the crucial growth step takes place long after deposition, the actual technique used to deposit the layer is of secondary importance. In in-situ growth, the film is deposited in crystalline form and, although it may need some low temperature annealing to achieve the correct oxygen stoichiometry, it requires no substantial rearrangement of the lattice after growth. In-situ growth has several advantages. For example, the lower temperature involved in in-situ growth minimizes contamination from the substrate. In addition, single crystal films can be grown with greatly improved physical properties and the film surface can be smooth. In this thesis, we studied relevant work in the field of high temperature superconducting YBCO thin films.This study include the pulsed laser deposition, fabrication of YBCO films and their characterization The physical phenomena involved in then interaction of high power nanosecond excimer-laser pulses with YBCO bulk targets resulting in ablation, plasma formation and subsequent deposition of YBCO thin films have been studied.

This thesis is organized in three main parts. Theoretical background and PLD system are discussed in Chapter 2 and Chapter 3. Experimantal methods involving

fabrication of YBCO thin films, PLD set up and measurement techniques explained Chapter 4. The main result on grown YBCO films are presented in Chapter 5. The thesis is summarized in Chapter 6.

CHAPTER 2

SUPERCONDUCTIVITY

2.1. Fundamental Properties of Superconductivity

Superconductivity means vanishing electrical resistance in a material below a certain critical temperature T_c (Figure 2.1). Experimental works showed that above a certain critical field H_c an applied magnetic field destroys the superconductivity. The critical magnetic field is a function at temperature such that it tends to zero when the temperature is close to T_c (Figure 2.4).

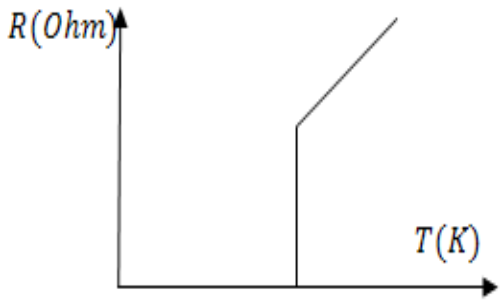

Figure 2.1. A temperature dependence of resistivity

The electrical current in superconductors flows without any resistance in the material and therefore lasts forever. At temperatures below the transition temperature T_c the magnetic flux is always expelled from superconductor regardless of the way in the magnetic field is applied. In other words when we apply an external magnetic field smaller than a certain critical field H_c, it is excluded by superconductor. This is called meissner effect or perfect diamagnetism.

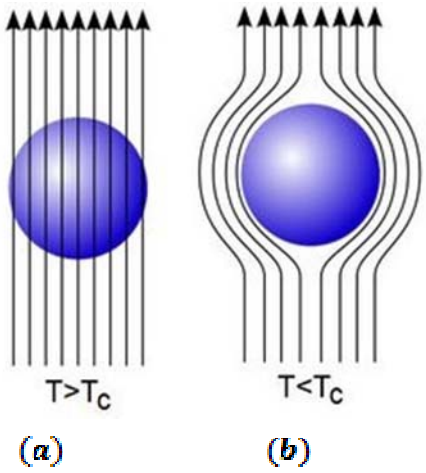

Figure 2.2. Diagram of the meissner effect (a) Magnetic field lines penetrate through a superconductor at $T > T_c$ (b) Magnetic field lines are excluded from a superconductor when it is below its critical temperature (Source: Wikipedia, 2010)

Assume that the superconductor is cooled down below the critical temperature in zero external magnetic fields. After that we apply an external field. The field does not penetrate the interior of the sample as shown in Figure 2.2. Actually, immediately after the field penetrates the surface layer of superconductor, an induced current is set up which, according to Lenz's Law, generates a magnetic field in the direction opposite to that of the external field. Hence the total field in the interior of the specimen is zero. Meissner and R. Ochsenfeld found that at $T < T_c$ the field inside a superconducting specimen was always zero. However at $T > T_c$, the resistivity of the specimen is finite and, therefore, the magnetic field penetrates into it .It is shown schematically in Figure 2.2.b (Meissner, 1933).

$$H_c(T) = H_c(0)\left[1 - \left(\frac{T}{T_c}\right)^2\right] \tag{2.1}$$

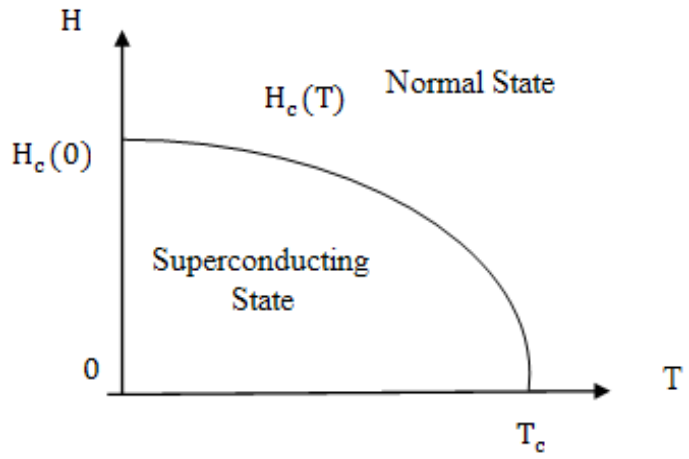

Figure 2. 3. The temperature dependence the critical field $H_c(T)$

Meissner effect is the most appropriate test for characterizating superconductors. In fact, even for an ideal superconductor, the magnetic field is not completely excluded but exists in a very narrow layer called penetration depth which is about 10^{-6}. The London penetration depth (λ_L) refers to the exponentially decaying magnetic field at the surface of a superconductor(. For temperatures $T \ll T_c$ λ_L is very small, at temperatures near T_c it reaches large values. If we apply the London equations to examine how a magnetic field penetrates a superconductor:

From Newton's Law, the equation of motion for a superconducting carrier with mass m and charge e in the presence of an electric field $\vec{E}$ is

$$n_s m \frac{d\vec{v_s}}{dt} = n_s e\vec{E} \tag{2.2}$$

Where $\vec{v_s}$ is the velocity of superconducting carrier and n_s is the number density of the superfluid.Taking into account that the supercurrent density is $\vec{j_s} = n_s e\vec{v_s}$, we get

$$\frac{d\vec{j_s}}{dt} = n_s \frac{e^2}{m}\vec{E} \tag{2.3}$$

$$\vec{E} = \frac{d(\Lambda\vec{j_s})}{dt} \tag{2.4}$$

$$\Lambda = \frac{m}{n_s e^2} \tag{2.5}$$

Where Λ is the London coefficient. (2.4) is known as the *first London equation*. Let us take the curl of both sides of equation (2.4) and use

$$\vec{\nabla} \times \vec{E} = -\frac{dB}{dt} \tag{2.6}$$

Maxwell equation (2.6). It gives

$$\underbrace{\frac{d}{dt}\left[\vec{\nabla} \times (\Lambda \vec{\mathrm{j}_\mathrm{s}}) + \mathrm{B}\right]} = 0 \tag{2.7}$$

Flux through an arbitrary area inside a sample with infinite conductivity stays constant.

$$\Lambda\left(\vec{\nabla} \times \vec{j_s}\right) + B = 0 \tag{2.8}$$

This is the *second London equation*. Taking the curl of the Maxwell equation $\vec{\nabla} \times \vec{B_s} = -\mu_0 \vec{j_s}$ we obtain

$$\vec{\nabla} \times \vec{\nabla} \times \vec{B} = -\vec{\nabla} \times \mu_0 \vec{j_s} \tag{2.9}$$

With the vector identity $\vec{\nabla} \times \vec{\nabla} \times \vec{B} = \vec{\nabla}\left(\vec{\nabla}.\vec{B}\right) - \vec{\nabla}^2\vec{B}$ and using $\vec{\nabla}.\vec{B} = 0$ and the second London equation;

$$\vec{\nabla}^2\vec{B} = \frac{\mu_0}{\Lambda} = \frac{1}{\lambda_\mathrm{L}^2}\vec{\mathrm{B}}$$

If we apply this equation to the superconductor with a magnetic field B_0 in the region,$x > 0$ eq. (2.10) has the solution

$$B(x) = B_0 e^{-\frac{x}{\lambda_L}} \tag{2.10}$$

$$\lambda_L = \sqrt{\frac{m}{n_s e^2 \mu_0}} \tag{2.11}$$

This London equation can be used for obtaining the description of Meissner effect in which the applied magnetic field decays exponentially inside the superconductor with the characteristic decay length of London penetration depth λ_L, T (temperature) dependence of λ_L empirical relation;

$$\lambda_L(T) = \frac{\lambda_L(0)}{\sqrt{1-\left(\frac{T}{T_c}\right)}} \tag{2.12}$$

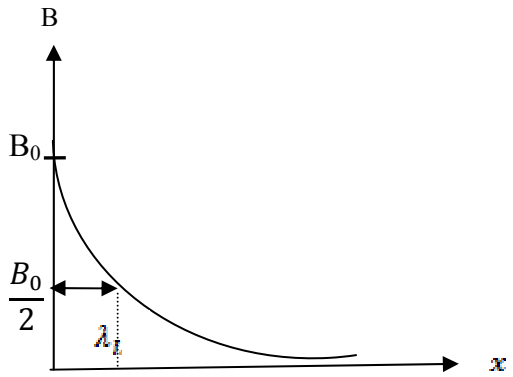

Figure 2.4. Schematic diyagram of the penetration of the magnetic field B inside the superconductor according to london equation

Superconductors are divided into two groups,namely type I and type II, according to their response to a magnetic field. Type I superconductors are characterized by expulsion of the magnetic field and by full diamagnetic behavior for all field values below H_c, at which the solid reverts to the normal state (the meissner effect). They have only a single critical magnetic field at which the solid undergoes a first order phase transition. This behavior is found most pure metals such as In, Sn, Hg…etc.

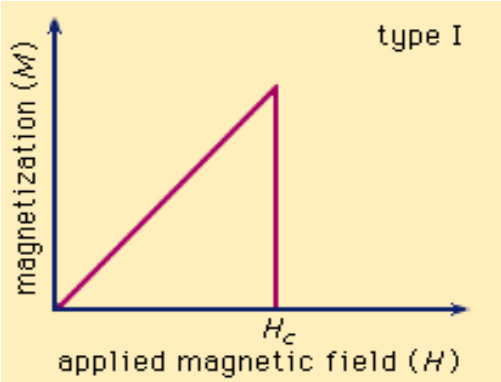

Figure 2.5. The reversible magnetic behavior of Type I superconductor

On the other hand, type II superconductors have two critical fields; the lower and the upper critical field which are H_{c1} and H_{c2} respectively. In type II superconductor the magnetic field does not penetrate the superconductor until it reaches the lower critical field $H_{c1}(H_0 < H_{c1})$. The average field in the interior of the specimen is $B = H_0 + 4\pi M$ is zero (meissner effect) that the type II superconductor is still a perfect diamagnetic. However, at $H_{c1} < H_0 < H_{c2}$, steadily increasing field B penetrates the superconductor and both the magnetic field and superconductivity coexist. This state is known as the *mixed state* of the type II superconductor. At a certain field $H_0 = H_{c2}$,, the average field in the interior, B becomes equal to H_0 and the superconductivity is destroyed.

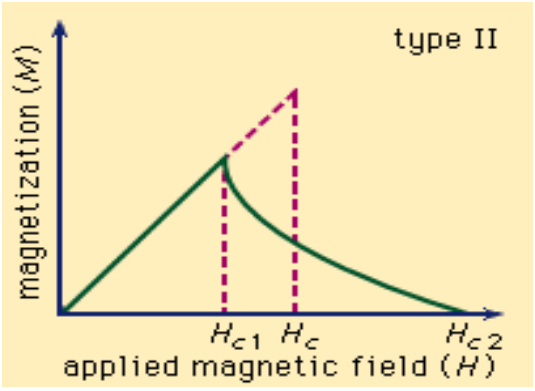

Figure 2.6. Type II superconductors have two critical magnetic fields which are and H_{c2} ; below H_{c1} type II behaves as type I, and above H_{c2} it becomes normal.

Above H_{c1}, the type II superconductor does not show the meissner effect. BeyondH_{c1}, in the so called mixed state, the magnetic field penetrates the material in

vortices which arranged forming hexagonal lattice. The magnetic flux enters a type II superconductor as fluxoids which consists of an integral number of a quantum known as fluxon. Each fluxon containing a single flux quantum (ϕ_0) given by

$$\phi_0 = \frac{h}{2e} = 2.07 \times 10^{-15} wb \tag{2.13}$$

The structure of a fluxon consists of a short-range (ξ) normal core surrounded by a long-range (λ) vortex of supercurrent. As the field increased further beyond H_{c1}, the density of fluxons increases. Eventually, when the internal flux density equals to the applied flux density at the upper critical field (H_{c2}), the cores of neighboring vortex overlap the sample goes to normal state.

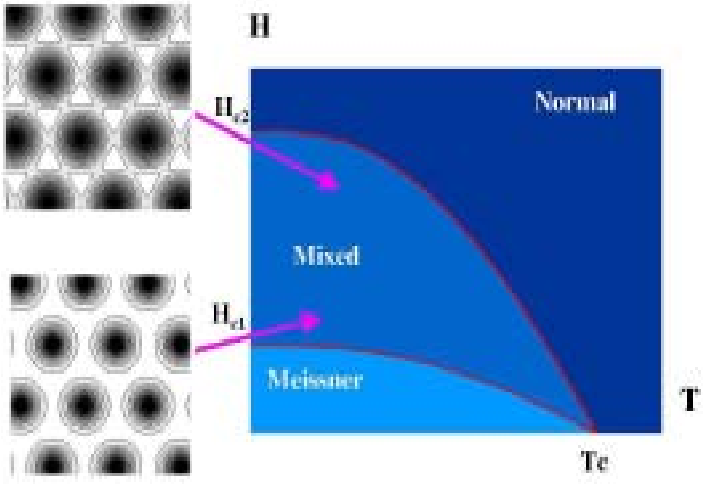

Figure 2.7. Schematic magnetic phase diagram of a type II superconductor
(Source: Poole, 1988)

If a current is flowing through the superconductor, in this mixed state, it produces a Lorentz force acting on the vortices. The flux lines start to move under the action of the Lorentz force at right angles to both the direction of the flux penetration and the transport current which is given by

$$\vec{F}_L = \vec{j} \times \vec{B} \tag{2.14}$$

However, there are some sorts of defects or impurities in superconductors, such as dislocation, walls, grain boundaries, voids, etc, in which the magnetic flux gets

trapped and which act as pinning centers for the vortices, keeping them. A schematic of the situation described figure 2.8, the fluxoids remain stationary, as long as there is present a flux pinning force at least equal to the Lorentz force $\vec{F}_L$ acting to move the fluxoids across the sample. This force resisting the fluxoid motion is called flux pinning force $\vec{F}_p$. When the Lorentz force on the fluxoids is greater than the pinning force, the fluxoid begin to move across the sample. The energy dissipated by drag or viscous for opposing this motion is supplied by the transport current. Hence, the movement of fluxoids causes resistive (there is a voltage drop along the specimen). This fluxoid motion is called flux flow and j_c is limited by the flux pinning in conductors, it is the source of the resistance observed at currents greater than the critical current.

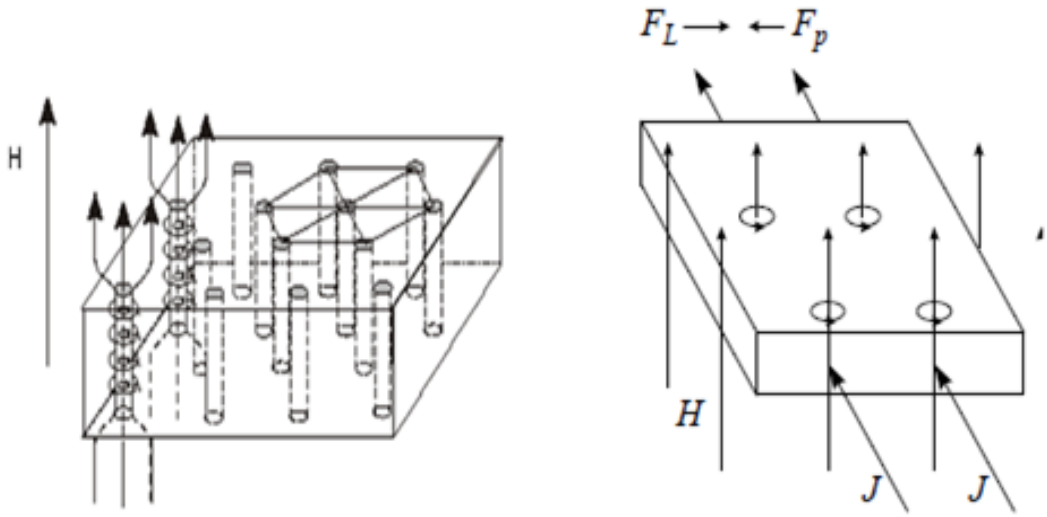

Figure 2.8. Mixed state in a Type II superconductor with the Abrikosov Lattice (Source: Abrikosov, 1957)

2.2. Superconducting Thin Films and Applications

The most important application areas of high-temperature superconductor materials are microelectronics components, superconducting wires, cables, and magnets. Microelectronics devices make use of HTS for detectors which measured magnetic flux and mm-wave radiation. In addition to this, HTS materials could be used to replace existing designs based on normal conductors. Compared to them, HTS components can be considerably cut down in size while their performance is improved. Since there are no electrical losses and power consumption in the components is low.

Applications of superconductors can be divided into two categrories which are electronic applications and electrical applications. Thin film technology is important in the electronic research in superconductivity. After a long period of development, there are many ways to prepare high-quality thin films by highly reproducible fabrication process such as moleculer beam epitaxy, sputtering, electron beam evaporation and laser ablation.

In develooing new superconducting electronics, one of the most useful actual device applications of high temperature superconductors is the superconducting quantum device (SQUID), the most sensitive for detecting magnetic fields. The SQUID is versatile in magnetic resonance imaging (MRI) and magnetroencephalography (MEG) in the medical diagnosis and industry application. The key parts of a SQUID are weak junctions called Josephson junctions which connect two superconducting regions. When a DC bias current is driven through the SQUID, an AC voltage is generated across the loop. This voltage is a periodic function of the magnetic flux through the loop. The SQUID is the leading commercial application of low temperature superconductor materials. The Josephson junctions for high-temperature SQUIDs can be fabricated, e.g., by etching a steep step edge on the substrate prior to the depositon, or by using a bicrystal substrate that consists of two parts fused together such that their crystal axes are rotated by a certain amount. In addition to this bolometers are resistance thermometers which are used as radiation detertors. Radiation heats the active part of the bolometer whose temperature increases. The temperature change is determined by measuring the resistivity of the absorber (bolometer). Superconducting bolometers make use of the large resistivity change at the superconducting transition.Another important application of high T_c superconductors is develop hybrid superconductor-semiconductor devices and systems. Hybridization such as the combination of superconductor and semiconductor devices in a single device, the combination of individual superconductor and semiconductor ddevices in a integrated circuit and the integration of superconductor circuits and semiconductor circuits into a complete system have ben designed for many years.

CHAPTER 3

YBCO AND PLD

3.1. YBCO

3.1.1. Crystal Structure of YBCO

The crystallographic structure of high temperature superconductors has been studied since their discovery for many research groups. Crystallographers classify the structure of these oxides as of perovskite type with CuO_2 planes lying normal to the crystallographic c-direction. This is a common feature of these materials, hense they are called cuprates. $YBa_2Cu_3O_{7-\delta}$ (YBCO) is the most well known high temperature superconductor, sometimes called the 1-2-3 compound. It was discovered in 1987 by Wu .It is transition temperature is nearly 92K. It is well above the liquid nitrogen barier (77K) and is relatively easy to synthesis. It is one of the members of the perovskite ceramic family. The Y-Ba-Cu-O compound usually exhibits a stoichiometry ranging from $YBa_2Cu_3O_6$ (non- superconducting) to $YBa_2Cu_3O_7$ (superconducting). Hence the fabricated YBCO compound usually exhibits an oxygen deficiency, δ. The material is always referred to as $YBa_2Cu_3O_{7-\delta}$ where $0 < \delta < 1$ (Jorgensen, 1990).

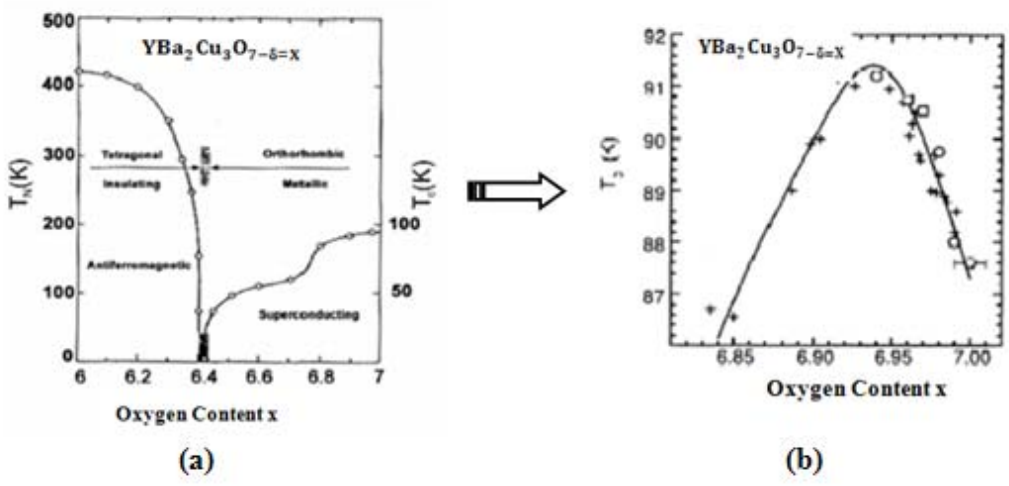

Figure 3.1. Phase diagram of $YBa_2Cu_3O_{7-\delta}$ system as a function of oxygen content and variation of T_c with oxygen content (Source: Poole, 1988)

The lattice structure is an orthorhombic with lattice parameters, a=3.82A^{o}, b=3.89A^{o}, and c=11.68 A^{o} along the (100), (010) and (001) directions when δ value is 0 or very small, whereas in case of δ=1 it becomes a tetragonal and non-superconducting. The oxygen content in YBCO determines the crystallographic structure Figure 3.1 and the hole concentration in the CuO_2 planes. For an oxygen content x=6 (where x=7-δ), the compound $YBa_2Cu_3O_6$ in the the tetragonal phase and it is an insulator. Increasing the oxygen content up to x=6.6 the compound undergoes a phase transition form tetragonal to orthorhombic. Finally, increasing x to 6.94, T_c approaches its maximum value (93K). Above x= 6.94, T_c decreases by about 4K as seen Figure 3.1. The maximum value found for T_c is due to an optimal hole dopng CuO_2 planes. The drop of T_c, when x exceeds 6.94, has been explained as being in overdoped state, when the holes in CuO_2 planes exceed the optimum concentration. The tetragonal phase observed at high temperatures in a range between 750^{o}C and 900^{o}C. On decreasing the temperature and increasing the oxygen content of the sample, by oxygen held and diffusion, a second-order phase transition occurs at about 700^{o}C from the tetragonal to the orthorhombic phase. If the structure of YBCO is orthorhombic, it is a superconducting transition temperature increases approxiamately up to 92K. The conductivity, critical current density J_c, as well as the unit cell parameter along ab-plane is different from those parameters along the c-axis. The conduction perpendicular to Cu- O sheet is very small. It is because the oxygen linking to the adjacent Cu-O layers in c-axis direction is completely absent.

As shown in Figure 3.1 and 3.2.a The orthorhombic structure of YBCO can be schematically represented as layered structure where three planes consisting in Cu and O atoms are inserted with two planes containing Ba and O and one plane containing Y. In the tetragonal phase Figure 3.2.b the oxygen sites in the base plane are about half accupied in the random manner, while in the orthorhombic phase they are ordered into Cu-O chains along the b-direction. The oxygen vacancies along the a-direction in the orthorhombic phase cause the unit cell to compress slightly so that $a < b$. Both the CuO_2 planes and the Cu-O chains in the orthorhombic phase contribute to the superconductivity. The CuO_2 planes include holes which are mobile charge carrier, and the Cu-O chains act as charge reservoirs that transfer holes the planes (Source: Poole, 1988)

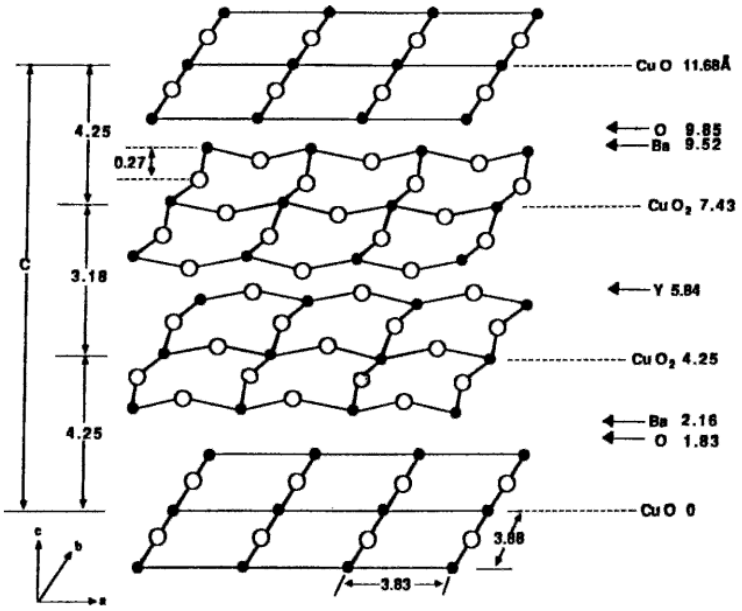

Figure 3.2. Layering scheme of orthorhombic $YBa_2Cu_3O_7$
(Source: Poole, 1988)

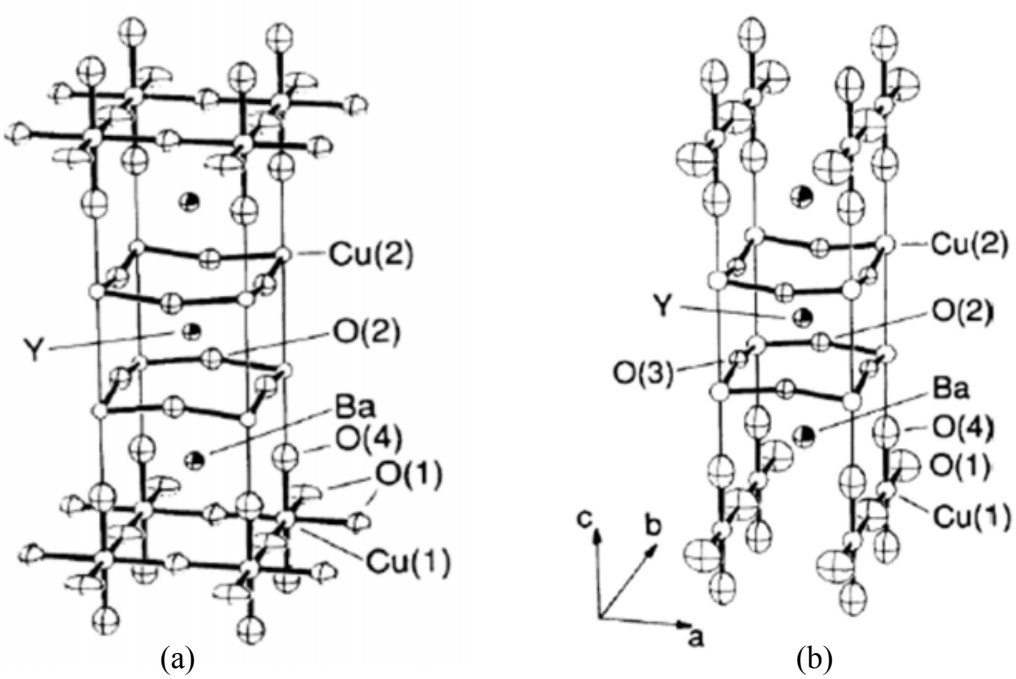

Figure 3.3. Sketches of the superconducting orthorhombic (a) and non superconducting tetragonal (Source: Jorgensan, 1987) (b) YBaCuO unit cells (Source: Schueller, 1987)

3.1.2. Physical Parameters of $YBa_2Cu_3O_{7-\delta}$

YBCO belongs to Type II of superconductors which are characterized by their ability to maintain their superconducting properties in very high magnetic fields. These superconductors accomplish this feat by a remarkable means. Instead of using the energy required to completely expel the magnetic fields, the fileds are limited to an internal aarray of normal-state flux tubes called vortices, for, they are surrounded by a circulating supercurrent.YBCO epitaxial thin films manage to carry relatively large current densities so they are used in device applications.

The surface energy of an interface between YBCO and normal regions is negative and hence the coherence length ($\boldsymbol{\xi}$) is less than the penetration depth ($\boldsymbol{\lambda}$). The coherence length might be thought of as a measure of the maximum distance between members of a Cooper pair and determines the distance at which lattice interruptions can disrupt the supercurrent. As a result, even twinnin planes or grain boundaries may have been sufficiently large dimensions to act as weak links explains the relatively low values of J_c seen in bulk seramic high-T_c superconductors. The penetration depth is a measure of the depth of surface layer of superconductor up to which the magnetic field penetrates. The values of coherence length, $\boldsymbol{\lambda}$ and some other physical parametersfor YBCO are given in Table 3.1.

The layered structure of the copper oxide superconductors leads to strong anisotropy in the normal and superconducting properties. The anisotrophy produces dramatic changes in properties in the (Source: Roul 2006) a-b plane, parallel to the layers, compared to the c direction, whih is perpendicular to the layers. The strong uniaxial anisotrophy can be seen in the normal state resistivity and magnetic susceptibility, and in the superconducting upper and lower critical fields. As listed in Table 3.1 the anisotropy is caused by differences in values of $\boldsymbol{\xi}$ and $\boldsymbol{\lambda}$ a long a-b plane and along c-axis (Nahum, 1991).

Table 3.1. Physical Parameters of $YBa_2Cu_3O_{7-\delta}$
(Source: Singh, 1989)

Parameter	Values
Transition Temperature	T_c=92K
Penetration Depth	λ(ab)≈1400A°
	λ(ab)~5x1400A°
Coherence Length	$\xi ab(0) = 15A°$
	$\xi ab(0) = 3 - 5A°$
Crystal Lattice Parameters	$a = 3.82A°, b = 3.89A°, c/3 = 3.89A°$
Thermal Conductivity	$3.2x10^{-2}Wcm^{-1}K^{-1}$(at 300K)
Specific Heat Capacity	0.39 J/gK
Reflectivity (at 248nm)	0.11
Solid Absorption Coefficient	$2.50x10^5 cm^{-1}$ (at 248nm)

3.1.3. Thin Films of $YBa_2Cu_3O_{7-\delta}$

Investigation on the electrical behavior of thin film materials have been stimulated largely by the endustrial demand for microminiaturized electronic components. The fundamental requirements for such a component are small size, high thermal, low cost, mechanical and aging stability, small value of surface resistance, low losses at a high-frequency and compatibility with the substrate used. These requirements can be fulfilled to a large extend by thin films of suitable material. For many significant applications of $YBa_2Cu_3O_{7-\delta}$ thin films in electronic devices, suitable substrates are necessary for achieving high-quality thin films.

3.1.4. Convenient Substrates for High-T_c Thin Films

The choice of substrates for high-T_c, thin films are very difficult as no ideal substrate for high-T_c superconducting materials available to date. According to first paper (Hollmann, 1996) which must be dealt with in determining the suitability of a substrate for a high-T_c film is the chemical compatibility of the two materials. This constraint is quite severe for high-T_c films, for, these materials are reactive with many technologically important substrates, such as Si, GaAs and Al_2O_3 at the temperatures required for the growth of high-T_c films. The substrate must also be compatible with deposition processes and all subsequent processing for the use of the films. In addition to this, regardless ofthe specific film growth method used, the substrate must be unreactive in the oxygen-rich ambient required for growth and processing. The other paper of concern in the selection of substrates for high T_c films is thermal expansion match. A decent thermal expansion match between films and substrates is essential to provide sufficient film adhesion and to avoid film cracking during thermal cycling.This requirement is more relevant because of the fragility of these materials.

The best high-T_c films grown to date, as determined by a multitude of metrics, including critical current density, morphology, and stability over time, are epitaxial on their substrates. Epitaxial growth requires the controlled crystallographic orientation of the film with respect to the substrate. In general, this requires matching of the film and substrate lattice parameters, atomic position, crystallographic orientation.The better match of all these parameters the more likely high quality epitaxial growth is to occur.

Other important things in the selection of substrates are size availability and cost, especially if the films are to be utilized commercially. Moreover, the substrate materials should have melting points below 2100^{o}C in an effort to be suitable for crystal pulling, which is the most appropriate technique for large-diameter-crystal growth. Using this, a list of properties desired in an ideal substrate is listed in table 3.2. For many significant applications of $YBa_2Cu_3O_{7-\delta}$ thin films in electronic devices, suitable substrates are necessary for achieving high-quality thin films. Substrates used for the high T_c thin films should have a good lattice match and chemically inert. At high temperature no chemical reaction with oxide superconductor occurs. Good thermal conduction and thermal match are important since stress and stain will arise from the thermal mismatch between the substrate and grown materials.

Table 3.2. Ideal Substrate Properties
(Source: Singh, 1989)

Desired property	*Reason*
Atomically smooth surface	Provide film uniformity and enable epitaxy
Perfect flatness	Provide mask definition
No porosity	Prevent excessive outgassing and improve film microstructure
Mechanical strength	
Thermal coefficient of expansion equal to that of deposited film	Prevent film stress Minimize film stress
High thermal conductivity	
Resistance to thermal shock	Prevent heating of circuit components Prevent damage and cracking during processing
Thermal stability	Permit heating during processing
Chemical stability	Permit unlimited use of process reagents
High electrical resistance	Provide insulation of circuit components
Low cost	Permit commercial application
Good lattice match	Maximize crystalline perfection

Moreover, the dielectric properties of the substrate have significant effect on high-frequency device performance. Appropriate dielectric properties and low value of loss tangent are important factors in microwave and high-frequency device applications. In order to successfully deposit film on substrate, the surface of the substrate must be smooth and flat. Otherwise, any surface irregularities on substrates result in degraded superconducting properties.

Substrates with low prices and large abound on the earth are beneficial for scientific research, investment and production. Substrates most used for thin film deposition are listed in table 3.3 and table 3.4 provides information that can be used to select substrates for the growth of high-T_c thin film for microwave devices for YBCO (Yamane, 1989)

Table 3.3. Properties of substrate materials for microwave devices of high-T_c Films (Source: Singh, 1989)

Material	ε	Tanδ	Chemical stability with respect to YBCO	Twinning	Mechanical Strength	Available Size(nm)
$SrTiO_3$	277	$6x10^{-2}$(l00K,300GHz)	Good	no	good	10x10
$LaGaO_3$	25	$6x10^{-3}$(l00K,500GHz)	good	yes	fair	40
$LaAlO_3$	23	$3 x10^{-5}$ (77 K,5GHz)	good	yes	fair	100
$NdGa0_3$	20	$3 x10^{-4}$ (77 K,5GHz)	good	no	fair	50
$YAlO_3$	17	$1x10^{-3}$(77K,10GHz)	fair	no	fair	30
$PrGaO_3$	24	$3.6x10^{-4}$(300K,1kHz)	good	yes	poor	10
MgO	9.65	$5x10^{-4}$ (100 K, 300	good	no	good	30x30
Al_2O_3	9.34	GHz)	poor	no	good	
YSZ	25	$3x10^{-5}$(77 K, 5 GHz)	good	no	fair	20x20
CeO_2	17	$8x10^{-3}$(l00K,300GHz)	good	no	fair	
$CaNdAlO_4$	17		good	no		30
$SrLaAlO_4$	17	$1x10^{-3}$ (77 K,100	good			25
$SrLaGaO_4$	22-26	GHz)				
$LiNbO_3$	23-44	$5 x10^{-4}$(100 K, 8 GHz)				
		$5 x10^{-5}$ (77 K, 5 GHz)				
		$2x10^{-3}$(300 K, 1 GHz)				

$SrTiO_3$ is one of the most widely used substrates for growing high T_c superconducting thin films. It posseses a perovskite structure and a good lattice match with YBCO. Therefore, YBCO can be epitaxially grown on it. $SrTiO_3$ also possesses a smooth, flat surface with high chemical stability and small thermal expansion mismatch with YBCO. But its large dielectric constant and poor high frequency properties make it unacceptable for microwave device applications.Furthermore, this substrate is considerably expensive. Therefore alternative substrates are necessary for mass production of microwave electronic devices. The other substrate MgO has received a good deal of interest in YBCO films deposition due to its modest dielectric constant, good thermal expansion when matching with YBCO and, availability. In this study, we used MgO substrates whose physical properties are given in detail in table 3.5.

Table 3.4. Physical properties of some oxide, metal and semiconductor substrates for the growth of YBCO superconducting films (Source: Singh, 1989)

Material	Crystal system	Lattice Constant(A^O)			Melting Point
		a	b	c	
$SrTiO_3$	Cubic	3.91			2353
$LaGaO_3$	Orthorhombic	5.52		5.49	2023
$LaAlO_3$	Rhombohedral	7.77			2453
$NdGaO_3$	Orthorhombic	3.79			1873
$NdAlO_3$	Rhombohedral	5.43		5.55	2363
$YAlO_3$	Orthorhombic	7.70			2148
$PrGaO_3$	Orthorhombic	3.75			1680
$GdAlO_3$	Orthorhombic	3.66		3.77	1940
$EuAlO_3$	Orthorhombic	3.69			2060
$NdAlO_3$	Rhombohedral	5.46		5.49	2070
$PrAlO_3$	Rhombohedral	7.74			2080
MgO	Cubic	3.73		3.72	3100
Al_2O_3	Trigonal	3.73			2300
YSZ	Cubic	3.73		3.72	3000
CeO_2	Cubic	3.73			2900
$SrLaGaO_4$	Tetragonal	3.75			1793
Ag	Cubic	3.76			961
Au	Cubic	4.20			1064
Cu	Cubic	4.73			1083
Pt	Cubic	13.00			1772
Si	Cubic	5.16			1685
Ge	Cubic	5.40			1231
GaAs	Cubic	3.84			1510
		12.68			
		4.07			
		4.08			
		3.61			
		3.92			
		5.43			
		5.65			
		5.65			

Table 3.5. Typical properties of single crystal MgO substrates
(Source: Singh, 1989)

Substrate	**MgO**
Crystal Structure	**Cubic**
Lattice Parameter (A^0)	**a=4.20**
Thermal Conductivity($WK^{-1}cm^{-3}$)	**3**
Thermal Expansion Coeff.(10^{-6})	**12.8**
Specific Heat($JK^{-1}cm^{-1}$)	
Reflectance@850 nm(%)	**0.53**
transmittance@850 nm(%)	**3**
Absorption@850 nm(%)	**89.5**
Melting Point(°C)	**7.5**
	2800

The lattice mismatch between MgO and YBCO is quite large ~9%. However, high quality epitaxial YBCO films can be successfully deposited on it under proper deposition conditions. The other disadvantage of substrate is that it reacts with water vapor. Another substrate is sapphire which is being interested as a substrate in view of its good high frequency properties and availability, but sapphire reacts readily with YBCO.

3.2. Pulsed Laser Deposition of $YBa_2Cu_3O_{7-\delta}$

After Venkatesan and co-workers successfully demonstrated *in situ* preparation of YBCO thin films with high critical temperature Tc and high critical current density Jc by the pulsed laser deposition (PLD) technique during late 1987 and early 1988 (Tallon, 1995), PLD has been widely used to prepare epitaxial thin films of any oxide material, including HTS materials. PLD is becoming one of the most important techniques to engineer thin film growth in research laboratories, because it has a number of advantages over most other deposition processes. The energy at the target can be controlled independently of the process pressure and gas mixture, and stoichiometric depositon can easily be contucted. High energy densities, high rates and

high process flexibility are characteristic features of the process. Furthermore, the method is fast and cost effective way to produce high quality films (Venkatesan, 1996).

The essential process of PLD consists of melting and evaporating of target materials with the pulsed laser beam. In PLD of YBCO thin films, a pulsed laser strikes target which is a solid bulk YBCO. Some of the target materials are removed, escaping in the form of a plume. Part of the plume comes in contact with surface of a heated substrate kept away from the YBCO target.The plume, which consist building blocks of the YBCO lattice, covers the substrate. The result is the fabrication of thin film of YBCO materials with the same chemical structure as the target. PLD offers numerous advantages, including film stoichiometry closed the target, high deposition rate, low contamination level and non-equilibrium processing. Moreover, accessible experimental parameter in PLD is very easy for the synthesis of high temperature superconducting thin films. These parameters are the substrate temperature, the energy of the atom flux, the relative and certain arrival rate of atoms for compound films and the pressure in the chamber.

3.2.1. Pulsed Laser Deposition System

The basic experimental design for thin film deposition by laser ablation is similar to other physical vapor deposition process. The apparatus includes a vacuum chamber, a substrate holder with presice temperature control (heater) and target. Figure 3.4 is a schematic diagram of a typical PLD system. An excimer laser which operates using a mixture of Kr, F_2, He, and Ne generates pulses with a wavelength varying from 193nm to 308 nm is used for target ablation. The laser fluence is varied by either varying the laser output energy or by focusing the beam.

The optical imaging system consists of a mirror and planoconcave lens. The mirror has reflective coating surface. The laser beam is passed into the chamber by a quartz window which is sensitive to damage if the laser energy density is too high or if the window is covered by dust particles. Chamber has several quartz windows, one to admit the laser beam while the others are for *in-situ* plasma diagnostics and monitoring the growth. The growth chamber contains substrate holder with heater bock, a rotating target holder and a shutter. The oxygen pressure during deposition is regulated using a mass flow controller and a microvalve.

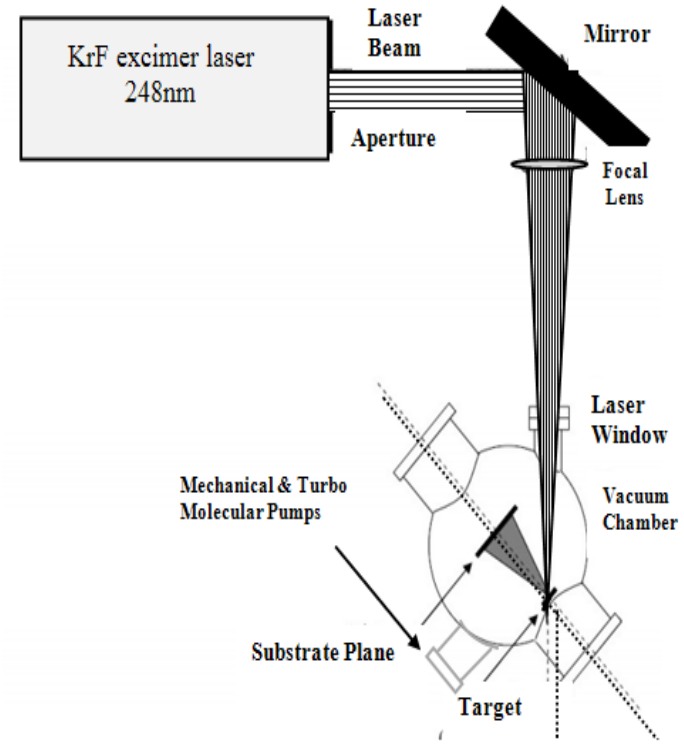

Figure 3.4. Schematic representation of PLD system

3.2.1.1. Laser-Target Interaction

Laser-target interactions can be described by the term sputtering. In termal sputtering surface temperature of the target is typically above boiling of the ablated material, but the rates of ablated material typically need even higher temperatures. Hence, thermal sputtering can explain the formation of the ablation cloud. Thermal process can be summarized schematically in Figure 3.5. The laser radiation is absorbed by the surface of the target where the photons energy causes surface heating. The increase in the surface temperature, which can easily exceed the melting point of ceramics ~1500^{o}C, depends on the optical penetration depth of the material, the thermal conductivity of the target and rate at which the photons are supplied. As the laser pulse continues to irradiate the target the molten surface layer is evaporated. Congruent evaporation, in which all the components of the target material are effectively released simultaneously, is achieved.Since the laser energy is supplied to a small volume in a short time nearly 18ns. This ensures that ejected material has the same stoichiometry as target material.

The thermal effects of pulsed nanosecond laser-irradiation of materials are determined by the laser pulse parameters (temporal power density *I(t)*, pulse duration tp, wavelength, etc.), optical properties (reflectivity *R*, absorption coefficient α), and the thermal properties of the material (thermal conductivity K, latent heat per unit volume L_v specific heat per unit volume C_v , ablation temperature T_v, etc.). The thermal diffusivity D = K/C_v, defines the thermal diffusion length $(2Dt_p)^{0.5}$ which determines the spread of the temperature profile during the laser pulses. The temperature in the target T(x, t) during laser irradiation is controlled by the heat flow equation given by (Wood, 1981)

$$C_v(T)\frac{\partial T(x,t)}{\partial t} = \frac{\partial}{\partial x}\left[K(T)\frac{\partial T(x,t)}{\partial Xx}\right] + (1-R)I_0(x,t)\alpha e^{-\alpha x} \qquad (3.1)$$

with appropriate boundary conditions which take into account the formation and movement of the solid-liquid (or liquid-vapor) interface. Here, x refers to the direction in the plane perpendicular to the target, t refers to the time. The second term on the right hand side of the equation is termed as the heat generation term due to the absorption of the incident laser beam by the target. If the surface of the material is highly absorbing (α =≥ $10^6 cm^{-1}$) to the incident laser beam, the heat generation term can be removed from Eq. 3.1, and applied to the front surface boundary condition.

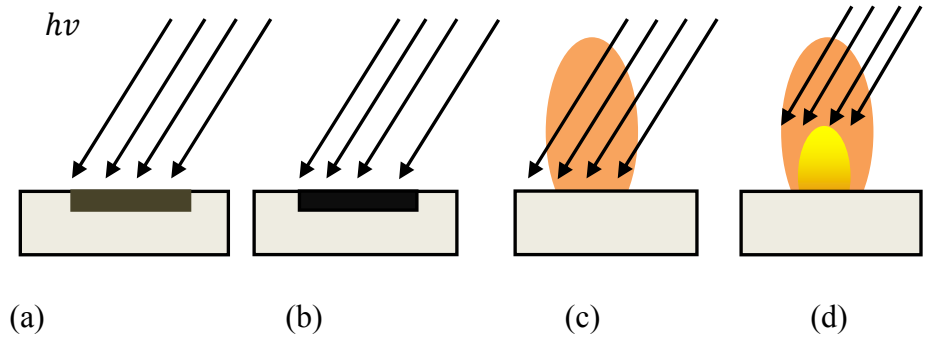

Figure 3.5. Schematic of laser –target interaction

a) Initial laser irradiation hits the target,
b) It melts the surface of the target,
c) The liquid is vaporized,
d) Then it is ionized to form plasma that is ejected from the target surface.

Briefly, laser-target interaction depends on the laser properties such as pulse duration, intensity, wavelength and the target properties such as the vaporization energy, absorption depth, specific heat, and thermal conductivity. Ablated materials due to laser-target interactions produce plasma which includes high energetic species.

3.2.1.2. Plume-Laser Interaction

Heating of the target by the high intensity laser beam causes electronic excitation of target atoms, ablation and exfoliation of the surface and plasma formation (Bär, 2004).This plasma absorbsfurther laser radiation by inelastic free electron scattering (inverse Bremstrahlung) which causes it to be heated. As the plasma enlarges the electron density decreases and the plasma becomes transparent to the laser radiation. In this way the behavior of the plasma self-regulates the laser-target interaction. Plasma can be determined as a quasi-neutral gas. It is formed when the content of particles such as electrons, ions, neutral atoms, molecules, molten droplets and large particulates in the vapor reach a critical value above the target. Because of the collision between these particles, we see a luminous plasma plume. The flux of ions and electrons as a function of temperature can be predicted by the Richardson's and Langmuir-Saha equations, respectively. Both of these equations show an exponential increase in the fraction of ionized species with temperature. Higher ionized fractions than predicted by the Langmuir-Saha equation have been observed in laser irradiated targets (Nakayama, 1984). This has been attributed to the higher temperatures induced by absorption of the laser beam by the evaporating material and electron impact ionization.

The physical mechanisms involved in the absorption and reflection of the laser energy by the evaporating material were identified in the early experiments as the sources for very high temperature (~1 KeV) plasma. The penetration and absorption of the laser beam by the plasma depends on the electron-ion density, temperature, as well as the wavelength of the laser light. For penetration (or reflection) of the incident laser beam the plasma frequency (vp) should be lower than the laser frequency.

At a local thermal equilibrium, the degree of ionization of the plasma as a function of density, temperature, and the ionization energies is determined by the Saha-

Eggert equation which can be derived from the Boltzman Distribution (Vankatesan, 1996):

$$\frac{n_e n_i}{n_n} = \left(\frac{Q_e Q_i}{Q_n}\right)^{3/2} \left(\frac{m_e m_i}{m_e + m_i}\right)^{3/2} exp\left(-\frac{\Psi_i}{k_B T}\right) \tag{3.2}$$

where n_e, n_i, n_n are the densities of electrons, ions and neutrons, *Qe, Qi, Qn* represent the internal partition functions of electrons, ions, and neutrals, ψ_i is the ionization potential of the neutral atom (Ho, 1996).

The degree of ionization depends on the laser parameters (such as wavelenght, fluence and pulse duration) and properties of target material. The Saha-Eggert equation is valid for weakly ionized plasmas for which the screening of the coulomb charge of ions and electrons is negligible. This condition can be provided when Debye length is sufficiently large**.**

Generally expansion of plasma is based on the evaporants from the target but sometimes this situation can occur differently. Because of the formation of a plasma in front of the target, the laser beam will be partially absorbed before it reaches the target.It is called "plasma shielding".Absorption of light in the plasma can be determined by two mechanisms preeminently that are inverse bremsstrahlung and photoionization of excited atoms (Chena, 2005) and the absorption coefficients for these two mechanisms are:

$$\alpha_{e-\alpha} = 2.90 \times 10^{19} n_e n_0 T_e^{3/2} G_{e-a}/v^3 \tag{3.3}$$

$$\alpha_{e-i} = 3.427 \times 10^{6} n_e{}^2 G_{e-i}/\left((T_h^{1/2})v^3\right) \tag{3.4}$$

where $\alpha_{e-\alpha}$ is absorption coefficient for electron-atom IB, α_{e-i} is the absorption coefficient for electron-ion IB, T_e and T_h are the electron and heavy-body temperatures, G_{e-a} and G_{e-i} are the Gaunt factors for electron-atom IB and electron-ion IB, v is the frequency of the laser pulse (Liu, 1995).

$$\alpha_{e-i} = 3.427 \times 10^{6} n_e{}^2 G_{e-i}/\left((T_h^{1/2})v^3\right) \tag{3.4}$$

$$\sigma = 7.9 \times 10^{-18} \left(\frac{E_i}{hv}\right)^3 \left(\frac{I_g}{E_i}\right)^{1/2} \tag{3.5}$$

,where σ is the cross section in photoionization, Ei is the ionization energy of excited state, $h\nu$ is the photon energy of laser pulse, I_g is the ambient gas ionization potential. (Liu, 1995)

Heating by IB occurs to absorb radiation when the expansion of plasma provokes an electron passing through the field of an ion. IB is the collisional absorbtion of energy so it increases energy and the temperature of electron. If the intensity of laser is necessarily high, the great plasma properties can be achieved by IB (Lunney, 1998). Photoionization is the other mechanism for absorption in which an electromagnetic radiation (photon) interacts with the target and ejects its electrons. Therefore it causes the target materal separated into charged particles**.**

During the ablation process of metals, the photonic energy from the laser radiation is combined with the target bulk. This situation brings about the ejection of macroscopic particulates and therefore it can cause hazardous effects on film growth (Willmott, 2000)

3.2.1.3. Plasma Expansion

Plasma expands freely and adiabatically in vacuum. It's perpendicular to the surface of the target. Because of the collisions between the particles in plasma, it's possible to see a weak light inside the chamber. During plama expansion, internal thermal and ionization energies are converted into kinetic energies of the ablated species (Mijatovic, 2004). For laser induced plasma, when there is a high pressure thermodynamic gas in chamber, the adiabatic expansion develops because of temperature dependency. During plasma expansion, temperature decreases. Also plume density reduces and inversely proportional cube of the distance from the target. This reduction causes a decrease in collision rate of particles in plume and is concluded with direct motion towards the substrate due to random kinetic energy of particles.

It is very important to use background gas in PLD experiments because it provides optimization of experimental parameters during the film production process (Chena, 2005)**.** Gases are generally used to thermalize the plasma species through multiple collisions and to condensate significant materials from the target trough ablation **(**Willmott, 2000**).** The expansion dynamics of the plasma highly depend on the

background gas pressure. Background gas can be a non-reactive or reactive gas. See Figure 3. 6 (Bär, 2004).

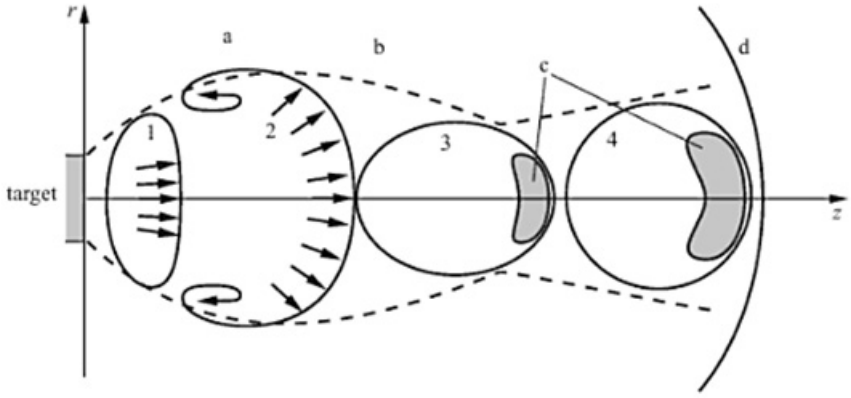

Figure 3.6. Stages of plasma expansion in backround gas environment: **a)** vertical motion arising at the plume periphery broken line **b)** motion of the plume boundary point farthest from the plume axis z **c)** regions with the pressure increase in front part of the plume **d)** shock wave ahead of the plume

The expansion of the plasma in the background gas environment begins with the movement of particles from the target and forming a particle cloud like a disk. The cloud becomes enlarge because of plume velocity distribution (positon 1). When the cloud pressure equals to background gas pressure, the plasma expands excessively (position 2). After overexpansion its size becomes smaller and pressure of plasma exceeds the pressure of the background gas (position 3). This situation results in the expansion of plume again at which it has the same velocity as the background gas in the shock front and finally expansion stops (position 4) **(**Bär, 2004). Therefore background gas in vacuum chamber slows down the plasma which results in the formation of shock waves and causes its confinement which leads to stop motion. Expansion in background gas atmosphere depends on the total energy of the plume and the ambient gas pressure.

To determine plasma expansion in the presence of background gas, the *"drag force "* and the *"blast wave "* models are commonly seen in literature (Afonso, 1990)**.** At low pressures the drag-force model describes the expansion of plasma. In this model the ejected species experiences a viscous force proportional to its velocity v through the background gas.

For the high background gas pressures, expansion mechanism can be described by blast-wave model. When plasma expands, it behaves as a piston so that it presses, squezes, and accelerates the gas molecules. Due to this piston effect gas molecules

reach supersonic velocities with the formation of the shock waves (Gammino, 2003). Shock wave formation is caused by the sudden release of energy and is observed in blast-wave model for high background gas pressures. In this model the propagation of shock waves are described through the background gas.

In PLD experiments both of these mechanisms are combined to explain expansion of plasma. At the beginning of the expansion it begins with the drag-force model at low temperatures then plasma starts to slow in order to form shock front through a background gas so it expands according to blast-wave model.

3.2.1.4. Plume Orientation

When the laser-generated plume goes towards the substrate, one must takes into account plume tilting.Because real targets are usually not perfectlyplanar and laser beam intensity profile on target may be skewed or non-uniform. Laser spot size, surface topography of target, laser pulse length, and wavelength affect the plume orientation. These factors have a small influence on the orientation except laser spot size. When the laser spot dimensions (diameter of the source) are much smaller than the target substrate distance, the angular distribution of the plume is determined by $\cos\theta$ law (Chrisey, 1994).

The maximum angular distribution of ions can be achieved when it is along the normal of the target. The maximum concentration of ions along the normal of the target in the form of a collimated beam is termed as forward peak which is commonly approximated by a $\cos^n\theta$ function and also emerge because of the collisions of plume species among themselves (Rafique, 2004). See Figure 3. 7:

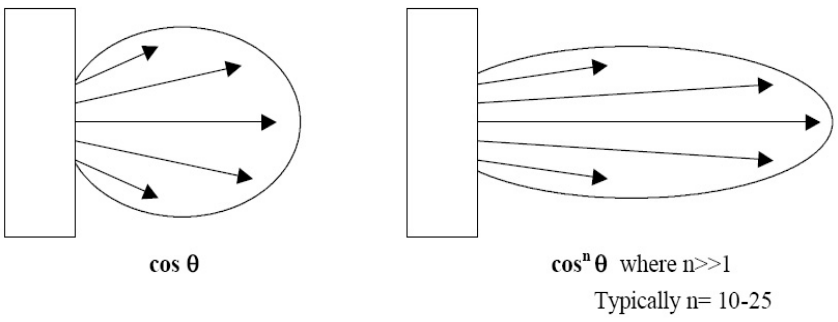

Figure 3.7. Shematic representation of plume angular distribution

Therefore the total orientation can be expressed as in below and generally this equation can be applied to all particles in plasma (Ohring, 1997):

$$acos\theta + bcos^n\theta \tag{3.6}$$

In the background gas environment is the angular distribution of plume extents. It is an advantage since narrow angular distribution of plume can cause contamination in chamber with respect to high deposition rate.

3.2.1.5. Nucleation and Film Growth

Ablated materials from the target hit the substrate. This bombardment results in sputtering of some atoms from the substrate surface. Particles from the target and the substrate create a collision region to provide condensation of them. When condensation rate is higher than the rate of sputtered particles, film begins to grow on the substrate surface.In this process when a particle condenses from vapor to solid, it may evaporate again or it may diffuse along the substrate which causes adsorption or re-evaporation of diffusing particles. More than one adsorbed particles can lead nucleation of clusters and the addition of these particles provide film growth (Lüth, 2001). See Figure 3.8 **(**Jaakkola, 2003).

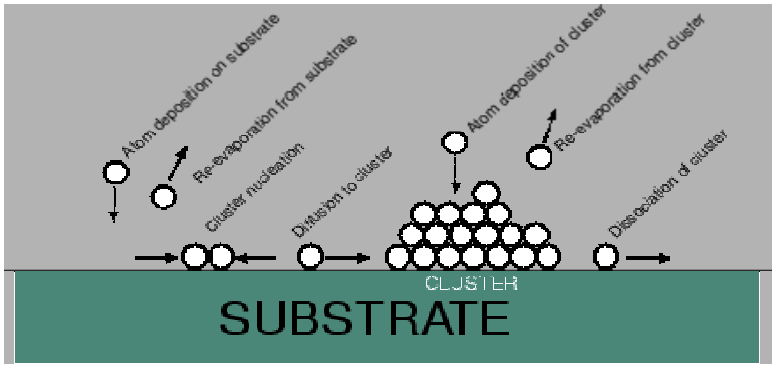

Figure 3.8. A diagram of atomic processes in the nucleation of three-dimensional clusters of deposited film atoms on a substrate surface

Some factors influence film growth such as density, energy, degree of ionization, type of condensing material, temperature, and nature of substrate. In PLD,

the growing film is usually not in thermodynamic equilibrium and kinetic effects have to be taken into account, which lead to the occurance of different growth modes (Satischandra, 2005). There are three types of thin film growth mode which are called island growth (Volmer-Weber, 3dimensional cluster), layer by layer growth (Frank-van der Merwe, 2dimensional cluster), and layer + island growth (Stranski-Krastanov). In layer-by-layer growth, nucleation of each next layer occurs only after the previous layer is completed. There is a stong bonding between the substrate and layer atoms in this mode.

This stage in PLD is very important because surface morphology of film depends on the nucletion and growth mechanism. Nucleation causes condensation of species from gas to solid phase and provides the creation of surface steps and subsequent growth causes lateral movement of these steps. When supersaturated gas phase is reached, the nuclei begin to form. The formation of nuclei depends on the activation energy. After a critical density is reached, the nuclei grow and crystallization begins to develop (Satischandra, 2005).

When a particle transfers from the gas phase to the condensed phase of the deposited film, it is determined by a Gibbs free enthalpy:

$$a\Delta G = n\Delta\mu \tag{3.7}$$

At equilibrium, particle must obey;

$$\mu_{solid} P_0(T) = \mu_{vapor}(p_o, T) \tag{3.8}$$

where P_0 (t) equals to equilibrium vapor pressure. But, if the particle changes from vapor to solid at a pressure P, the free entalphy changes:

$$\Delta G = n\Delta\mu = nkTln(\boldsymbol{\xi}) \text{ where } \boldsymbol{\xi}=\frac{P}{P_0} \tag{3.9}$$

Where $^{p}/_{p_0}$ is called the degree of supersaturation.

Nucleation and growth mechanism depends predominantly on the supersaturation. Layer-by-layer growth is favored with increasing supersaturation. Small supersaturation causes large nuclei. In this condition islands are created then

grow and caolesce on the substrate surface. On the other hand when the supersaturation increases, the critical nucleus begins to shrink and lastly its shape transforms into a two dimensional layer from its first shape that is like a cap.Also another important parameter is substrate temperature. Many nuclei from under high evaporation rates generally have low probability to grow on the substrate if the substrate temperature is low and it causes fine-grained film. On the other hand atoms can be frozen and so they stick on the substrate due to low substrate temperature. This condition does not allow the surface diffusion and it can cause amorphous or disordered film. When the temperature is high, if there are a few nuclei, a coarse-grained film occur (Ohring, 1995).

It is possible to see growth diagram for films from R-T dependence of N99. It is the mean thickness at which a growing, thin and discontinuous film is given by the equation (Metev, 1989)**.**

$$N_{99} = 0.5\left(\frac{vN_0}{R}\right)\exp\left(\frac{-3E_{des}+2E_{sd}}{3kT}\right) \quad (3.10)$$

where v is the adatom (vapor atom) vibrational frequency, N_0 is the density of absorption sites on substrate, $E_{des}$is the activation energy for adatom desorption, $E_{sd}$is the activation energy of adatom surface diffusion. By observing growth diagram, low and high islands growth regions can be seen.

3.2.1.6. Macroscopic Particulate Production

The ejection of macroscopic particulate are called “laser droplets” which are caused by photomechanical effects and forces due to laser-induced stress between bulk metal and plasma. Also hydrodynamic sputtering intends forming of droplets at the target due to transient melting and after melting there are some roughness that occurs at the target surface. These laser droplets on the film surface can severely deteriorate the film quality and morphology. Laser droplets provoke 3 challences: subsurface boiling, recoil ejection and exfoliation (Willmott, 2000)

In order to prevent splashing, a velocity selector as a particle filter can be replaced between the target and the substrate to remove slow particles. Experimental results are the evidence of the utility of the velocity filtration (Pechen, 1995). YBCO

films are studied by electron microscopy is shown in figure. In Figure 3.9.a the surface of the film is covered with laser droplets without using particle filter. In Figure 3.9.b, laser droplets disappear owing to particle filter.

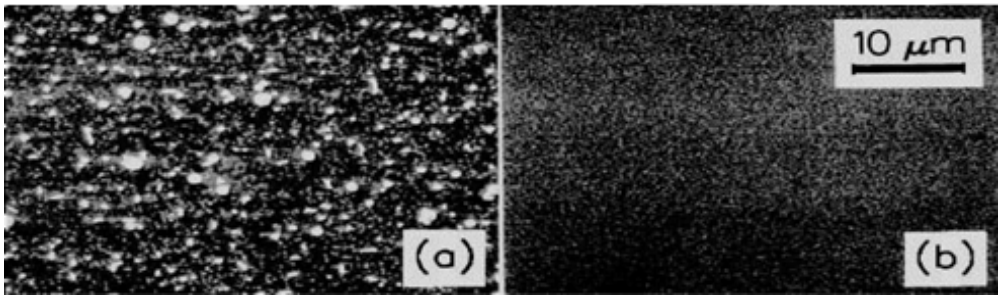

Figure 3. 9. Surfaces of YBCO films prepared on MgO substrates without **(a)** and with **(b)** velocity filtration of the laser-induced streams

The other avoidance method is to use smooth and dense targets or liquid target (Krebs, 2003) Also, positon of target or laser can be changed to achieve the best geometry for avoiding splashing and laser droplets. The convenient geometry can be achieved by putting substrate parallel with respect to the axis of the expanding plasma cloud. Therefore, heavier droplets pass when atomic and ionic species are deposited because of the collisions with molecules of the background gas. Another method is reduction of laser energy density (Doughty, 1995). By using these methods films can be growth without laser droplets.

3.2.1.7. Atomic Oxygen and Processing Geometry in the Growth of $YBa_2Cu_3O_{7-\delta}$ Films

Since atomic and ionic species ar more reactive compared to their molecular counterparts, it seems to be quite possible to obtain good quality YBCO films at lower in situ growth temperature by supplying a flux of atomic oxygen to the lattice of YBCO right during its formation. This concept has,in fact, been used by some PLD research groups to grow good quality YBCO films at relatively low deposition temperatures (Zheng, 1989) Singh have reported that an oxygen jet placed near YBCO target during PLD produces a strong atomic beam which results in the formation of YBCO films at lower temperatures than used for the growth of YBCO films in absence of such atomic

beam. According to Singh, the location of oxygen nozzle (i.e., whether it should be near the target or near the substrate or in the middle of target-substrate, please see Figure 3.11) also plays very crucial role in oxygen-incorporation to the film. The effect of oxygen-jet geometries on the superconducting quality of YBCO films have been presented in Figure 3.11 which shows the YBCO films obtained by positioning the oxygen-jet towards the substrate has higher T, than that of YBCO films obtained by positioning the oxygen-jet towards the target. The oxygen nozzle located near the target may generate more atomic or ionic oxygen, but such geometry is likely to interfere unfavorably by thermalizing the ablated species (Singh, 1989). The positioning of oxygen nozzle near the substrate assists the incorporation of oxygen during the film growth. A minute observation of the experimental set-up in these studies reveals that the oxygen jet was pointing in the same direction (i.e., towards the substrates) even though they were located at different position. Thus, what appears to be important and unambiguous is the generation of atomic oxygen which enables one to grow YBCO films with good quality at lower temperatures.

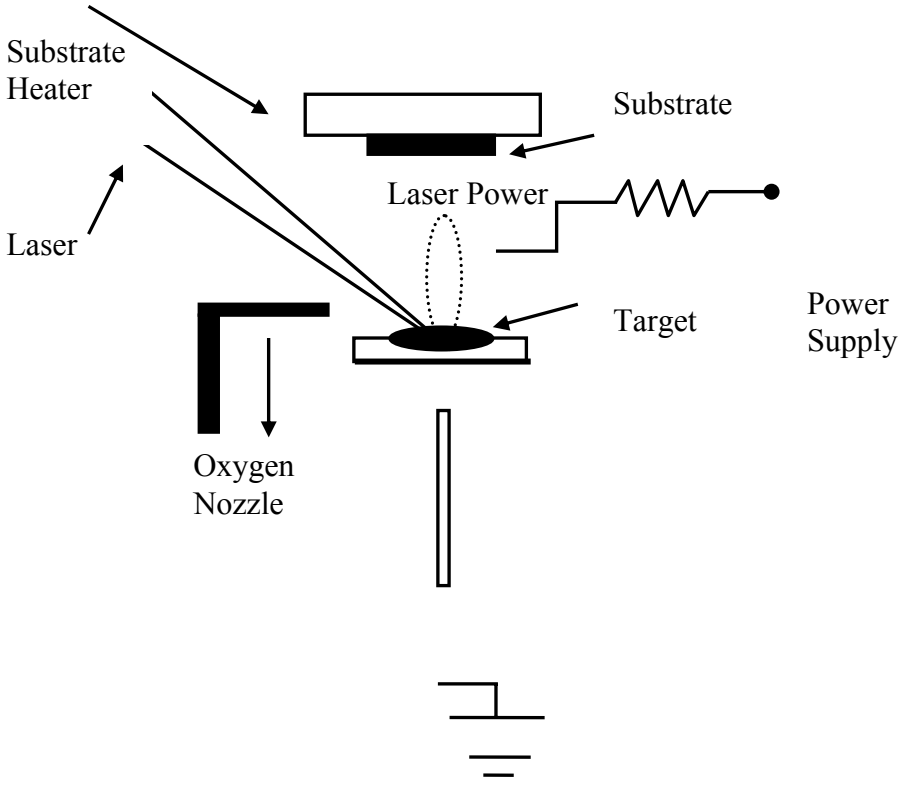

Figure 3.10. Schematic diagram of the laser deposition method showing the layout of the oxygen-jet directed differently

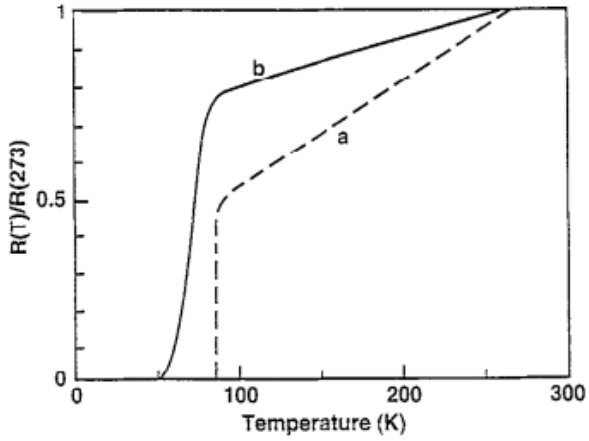

Figure 3.11. Normalized resistance vs. temperature plots for (a) YBCO film obtained while oxygen-jet was pointing towards the substrate (b) YBCO films obtained while oxygen-jet was pointing towards the target during laser deposition (Source: Singh, 1989)

CHAPTER 4

EXPERIMENTAL

4.1. YBCO Target Preaparation

In this study, we prepared a YBCO target.The sample was a mixture of Y_2O_3, $BaCO_3$ and CuO which were mixed in ratio of Y: Ba: Cu = 1:2:3.

$$0.5(Y_2O_3) + 2(BaCO_3) + 3(CuO) \rightarrow YBa_2Cu_3O_{7-\delta} + 2CO_2 \qquad (4.1)$$

This mixture was intimately mixed by grinding either in an agate ball mill or by grinding in agate mortar. The grinding times were of the order of 30 minutes to one hour until it was the uniformity of particle size. Tube furnace was used. The grinded material was as first step to calcine as loose in Al_2O_3 crucible at 920º C in air. This took 24 hours. After cooling to room temperature the black product was regrinded.when a big pellet pressed under pressure of 80 pa was made having diameter 25mm and thickness 3mm, this pellet was put for last sintering at 930º C for 48 hours with several intermittent regrindings. The cooling after the last sintering step and the subsequent heat treatment were always performed in an oxygen atmosphere. The $YBa_2Cu_3O_{7-\delta}$ sample resistance at room temperature was $11 - 35\Omega$. Polycristalline superconductor $YBa_2Cu_3O_{7-\delta}$ was characterized by various methods, such as Meissner effect x-ray diffraction and EDX.

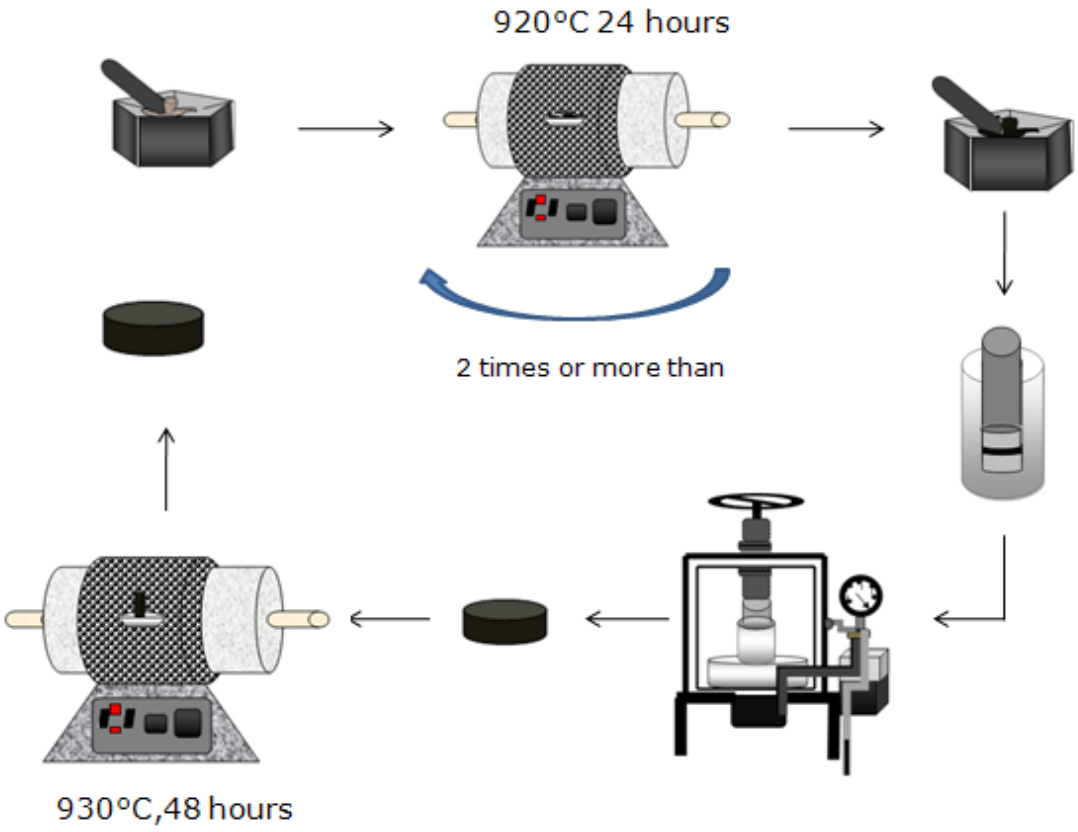

Figure 4.1. Target Preparation

4.2. YBCO Thin Film Deposition System; PLD

A new PLD system was set up with up a multi-target capability with a Neocera 6 multi-target carrousel. The light source used for these deposition experiments was a KrF excimer laser with dielectric rare mirror for 248 nm and uncoated MgF_2 window for all wavelengths. The laser has a wavelength of 248 nm, which is very effective for congruent ablation within 25 nm range. Tested pulse energy is 145 mJ, but we use that during deposition pulse energy is between 70 mJ and 100 mJ for low energy density. The energy density is varied by either laser output or beam size on the target. Laser beam dimensions are $11x7mm^2$ and can be adjusted by means of demagnification.The laser beam was focused by two perpendicularly assembled cylindrical lenses, situated outside the chamber. The focused laser beam was 45^o from the target normal, and the plume was generally perpendicular to the target surface. The energy loss from laser to lenses is 25%. The loss of the residual energy at the lens and the window is nearly 10%.

The total energy loss approximately is 37.5%. Pulsed duration is 18 ns of FWHM (full width at half maximum) and a pulse repetition rate is 5 Hz for our parameters.

Vacuum chamber provides base pressure nearly 10^{-6} torr with a turbo molecular pump. The maximum pressure drop is 10^{-8} with it. The oxygen pressure of the chamber is controlled by valve controllers (fine, coarse, target), a flow metering valve. The multi-target capability up to six targets allows producing many different compositions in a single deposition run to arrive at optimum composition having the desired material properties. There are two shields between the target and the substrate. One is a fixed shield which is protecting the other targets on the carousel from contaminations during the ablation of the active target. The other shield is working as a shutter and it is located in front of the substrate. Its function is to protect substrate by blocking the plume when target cleaning (preablation) or target changing during deposition. The conductive heater is attached in the vacuum chamber, which has maximum temperature 950^{o}C with temperature controller. Heater and substrate holder are placed in front of target.In addition, target change and rotation can be controlled automatically by program provided by Neocera.

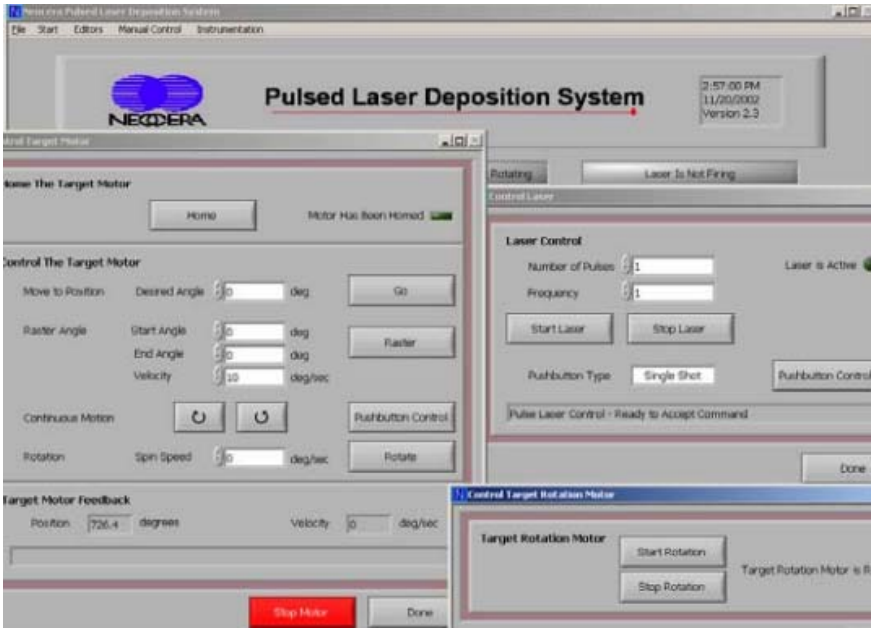

Figure 4.2. Control Window for Neocera PLD automation package

Writen programe as below:

Firstly we opened Neocera PLD page. After target raster angle, velocity, substrate holder velocity, shutter angle were entered from routine editor.

These parameters are;

- Target
  - Desired angle: 0
  - Start angle: 15^{o}
  - End angle: -15^{o}
  - Velocity: 47^{o}/s
  - Rotate: 11^{o}/s
- Substrate
  - Home offset: 180^{o}
  - Velocity: 25^{o}/s
- Pulse
  - Number of pulse: 900 shot ; preablation, 15000 shot; deposition.
  - Repetition Rate : 5hz
- Shutter Position
  - Closed: 48^{o}
  - Open: 20^{o}
  - For loading: 100^{o}
  - Velocity:10^{o}/s

After entered these parameters, we wrote two routine programm which are *preablation 900s 5Hz YBCO-X on MgO/$SrTiO_3$ raster from 15 to -15 sub.vel 25 shutter closed* and *deposition 15000s 5Hz YBCO-X on MgO/$SrTiO_3$ raster from 15 to -15 sub.vel 25 shutter opened.* As soon as we finished routine program, we opened loop editor to load program which was written.

Add line
Edit line
Load file
Select *preablation 900s 5Hz YBCO-X on MgO/$SrTiO_3$ raster from 15 to -15 sub.vel 25 shutter closed*
Update Change
Add line after
Edit line
Load file
Select *deposition 15000s 5Hz YBCO-X on MgO/$SrTiO_3$ raster from 15 to -15 sub.vel 25 shutter opened*

Update Change, Save

Write programme name.

Return the main Neocera PLD page and load program

Start Program.

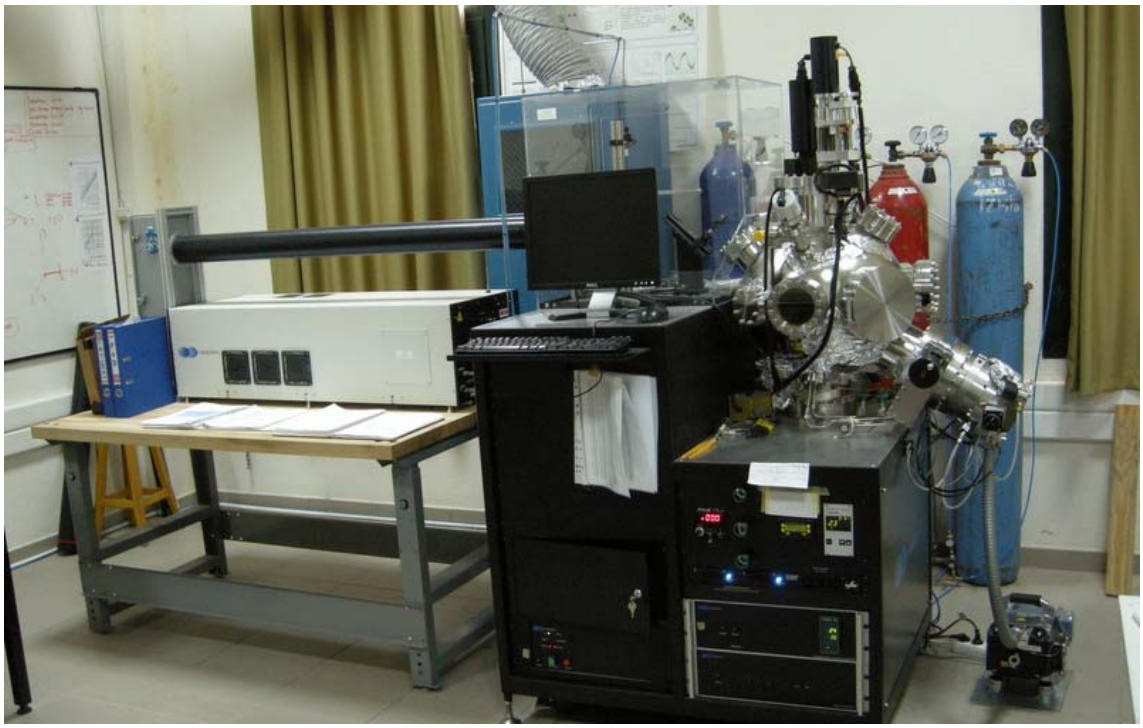

Figure 4.3. The schematics of the PLD set up used for this work

4.3. YBCO Thin Film Deposition

The substrates used in this work were mainly MgO (100) and single-side polished to average roughness Ra<1nm. The selection of MgO substrate was because of their modest dielectric constant, good thermal expansion. The substrate size was 5x5x0.5mm and cleaned with various chemicals. Respectively it was cleaned with acetone and alcohol in an ultrasonic cleaner nearly 45 minutes. After drying with pressurized nitrogen the substrate was laid on top of a small drop silver paste placed at off axis of the substrate plate and we waited that the silver paste spread easily to the edges of the substrate thanks to its weight. Before put the chamber, possible dust particles was removed from substrate using pressurized nitrogen. MgO has received a good deal of interest in YBCO films deposition due to its modest dielectric constant,

good thermal expansion when matching with YBCO and, availability. The lattice mismatch between MgO and YBCO is quite large ~ 9%. However, high-quality epitaxial YBCO films can be successfully deposited on it under proper deposition conditions. The other drawback of MgO substrate is that it eacts with water vapor. Hence, we conserved it from air contamination and water. The distance between target and substrate was 75 mm. The deposition chamber was filled with nitrogen and the plate was slid into the tracks of the substrate heater. At this point, one should check the condition of the target such as raster angle and its velocity. Pld system was pumped by two different vacuum pumps which are a rough pump and a turbo molecular pump. The Rough pump that is a mechanical pump, can pump down from atmospheric to 10^{-4} torr and the turbomolecular pump reduces the pressure 10^{-8} torr. Before the deposition, the vacuum is usually better than $5x10^{-6}$ torr. The Oxygen was used as background gas. After putting substrate and target, we waited that the base pressure was $3x10^{-6}$ torr. When the heater reached approximately at $800^{o}C$, we waited 30 minutes, for the substrate temperature is homogeneous.

The two step growth which are preablation and deposition were done. The first step is preablation to remove contamination of target surface that is cleaning target (number of pulses 900 shot and repetition rate 5 Hz). It taked 50 minutes (the number of pulses 15000 and repetition rate 5 Hz). The background gas pressure 300mtorr during the preablation and the deposition are controlled both upstream and downstream, with a pin valve on the Oxygen delivery and with the adjustment of the gate valve on the pumping port, respectively. In this way, a robust control of pressure inside the deposition chamber can be achieved within a wide range. In preablation step, the shutter closed and laser energy density is $1.83J/cm^2$. After this process, the shutter was opened and at the same pressure deposition was started. The deposition recipe for YBCO on the MgO substrates thin films is showed Figure 4.5 the deposition started by turning on the laser at the selected pulse-repetition rate (5Hz). The laser-spot position on the target was directed towards off axis position on the deposition plate. The colour, the shape of plume and the colour depend above all on the oxygen pressure. The deposition time was 50 minutes and according to deposition time its thickness according to deposition time is approximately 0,08nm/s. After the deposition process, the laser was switch off and post annealing begins. This step is necessarily to allow the formation of the superconducting lattice configuration. The TMP pump was switched off and the oxygen pressure is slowly increased to nearly 400-500 torr. The temperature of the deposition

plate decreased from 800°C to 550°C by 10°C/min. The system was hold in this state for an hour to ensure sufficient oxidation of the film. After annealing, the heater decreased to room temperature. The heater and the targets had to be cooled down for several hours. The chamber was filled with nitrogen. The substrate was removed from the plate.The film was stored in a small plastic box and it was put in desicator to prevent contamination of air.

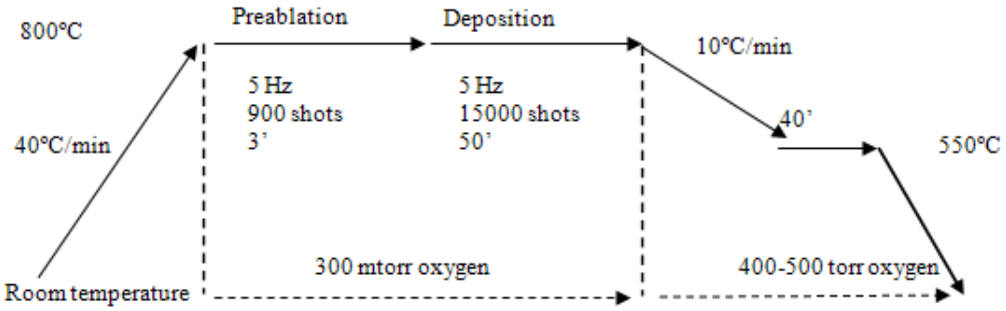

Figure 4.4. Deposition recipes for YBCO films on MgO

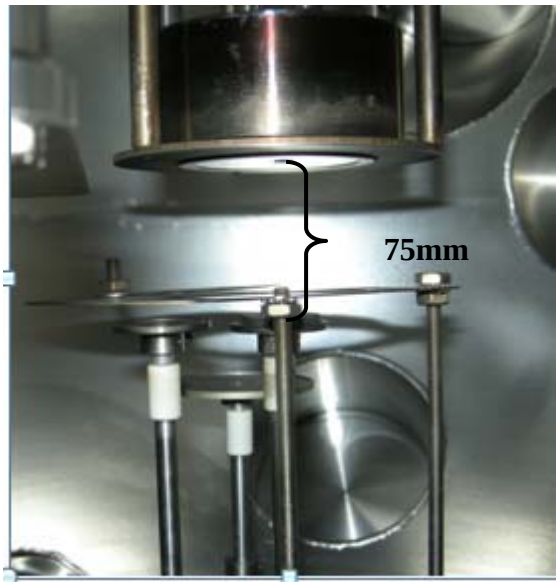

Figure 4.5. Distance between target and substrate.

Figure 4.6. Plume ejected from YBCO during deposition process

4.4. Characterization and Measurements

During this work, film quality immediately was tested by measuring resistance at the room temperature after the film was grown and removed from vacuum. The resistance changed from 250Ω to 700Ω. Transition temperature was measured by R-T measurement in the cryostat. To designate transition temperature of the prepared YBCO thin films, four-probe method was used. Fabricated films are characterized by x-ray diffraction (XRD), scanning electron microscopy (SEM), atomic force microscopy (AFM) and energy-dispersive X-ray spectroscopy (EDX) in an effort to analyze crystal structure, surface morphology and elemental composition to decide the deposition parameters.

4.4. 1. Scanning Electron Microscopy (SEM) and Electron Dispersive X-Ray (EDX) Analysis

The scanning electron microscopy (SEM) technique, which is a type of electron microscopy, was used to determine the microstructure of the films to know information

about surface morphologies of the grown films on MgO substrates. This technique is very usefull for a quick assessment of the entire surface area of a given film, whereas other, perhaps more sensitive methods (AFM) are somewhat slower and allow examination of only limited area of the sample. Using characterization our films by SEM, we had deposition parameters changed such as repetition rate, deposition time. Distance between target and substrate. In addition to this after film deposition and prepare YBCO target, Electron Dispersive X-Ray (EDX) was used to learn the chemical contents of them. Y, Ba, Cu, O contents were detect By EDX. According to collected EDX data we decided how long the film exposure oxygen.

SEM works with electrons instead of light. These electrons are liberated by a field emission source under high voltage. The incident electrons cause low-energy secondary electrons to be generated and some escaped from the surface. The secondary electrons emitted from the sample, the angle and velocity of these secondary electrons relating to the surface structure of the object are detected. A detector catches the secondary electrons and produces an electronic signal. This signal is amplified and transformed into a video scan-image that can be seen on a monitor or to a digital image.

4.4.2. X-Ray Diffraction (XRD) Analysis

X-ray diffraction (XRD) has been proved to be a valuable technique for the structure characterization of materials. The X-Ray Diffraction method was used in our study to define the crystal structure of the YBCO films. 2θ diffraction scan, which can give information on the phase, orientation and lattice parameters of the thin film under test.These films grown on MgO substrates and YBCO target were scanned in from $2\theta = 5°\text{C}$ to $80°C$. Using XRD results, we had deposition parameters changed whether the oxygen was enough at grown YBCO films on MgO or not.

4.4.3. R-T Measurements

The critical temperature, where the superconductor loses all resistance to the flow of electrical current, indicated that the material might be a superconductor. To measure R-T we used (He closed cycle) croyostat decreased in 4K. Determine the

critical temperature of the sample a four-point method was used for R-T by Teknis Firm.

Dc resistance was characterized by four-point probe technique to measure R vs T. Four electrode probes were placed on the surface of the thin film. The cryostat chamber was evacuated to $5x10^{-5}$ torr and the temperature was cooled down from 300K to 4K by a helium gas compressor. A constant current source was attached to the outher contacts with silver paints with a 10μA agitatin current, while the voltage drop between the inner contacts were measured via a nanovoltmeter. It was measured by KEITHLY 2400. After putting film in the cryostat, it was pumped by vacuum pump. We waited that the vacuum decreased in below $5x10^{-5}$ torr. As soon as the pressure was in the range of 10^{-5} torr, the cooling was started. It took about 3 hours to bring the sample to the minimum temperature, 4K. Firstly we set point at 290 K to make equal temperatures which belong to sensor A and sensor B thermometers. Otherwise, while the apiezon was initially cooled as temperature controlled might not be good. After the temperature was decreased in 4K, it increased to 100K. We collected data from 100K to 4K and from 4K and 100K. In order to accurately measure R-T of the our films, the temperature was increased by 0.1 K per 15 seconds by a labview program. In this measurement, resistance vs temperature, transition temperature, T_c, of superconducting materials can founded.

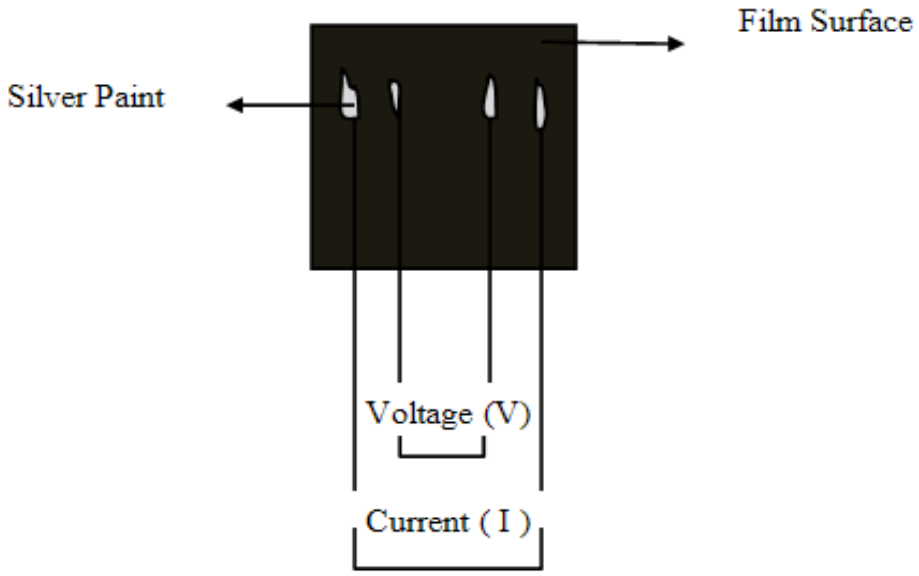

Figure 4.7. Schematic of four-point contacts

Operation of R-T measurements:

- **Lakeshore**
  - File
  - Open log: write name
  - Applied current:0,000010A
  - Configuration
  - Set point: 5K
  - Configurate
  - Ok
  - Measurement
  - Start
  - If the operation was completed, pressed Finish.
  - Stop
  - If the operation was not completed, pressed continue measurement
  - Configuration
  - Heater range: high
  - Set point: 100K
  - After the operation finished, set point: 297K, Stop.

CHAPTER 5

RESULTS AND DISCUSSION

In this study, with the objective to understand the special phenomena observed in the thin films samples, the YBCO thin films were characterized by using several techniques to gather the information on crystal structure, electrical properties and surface morphology. These results would be very helpful for understanding the properties of the YBCO thin films on MgO substrates.

5.1. XRD Results

X-ray diffraction analysis at room temperature using CuK_{α} radiation were performed to identify the crystalline phase existing in the time dependence annealed samples. The crystal structure of YBCO thin films prepared by PLD system were investigated by XRD. In the beginning of our study, Y_2O_3, $BaCO_3$ and CuO powders were used to produce target. The x-ray diffraction pattern of YBCO target is c-axis orientated.

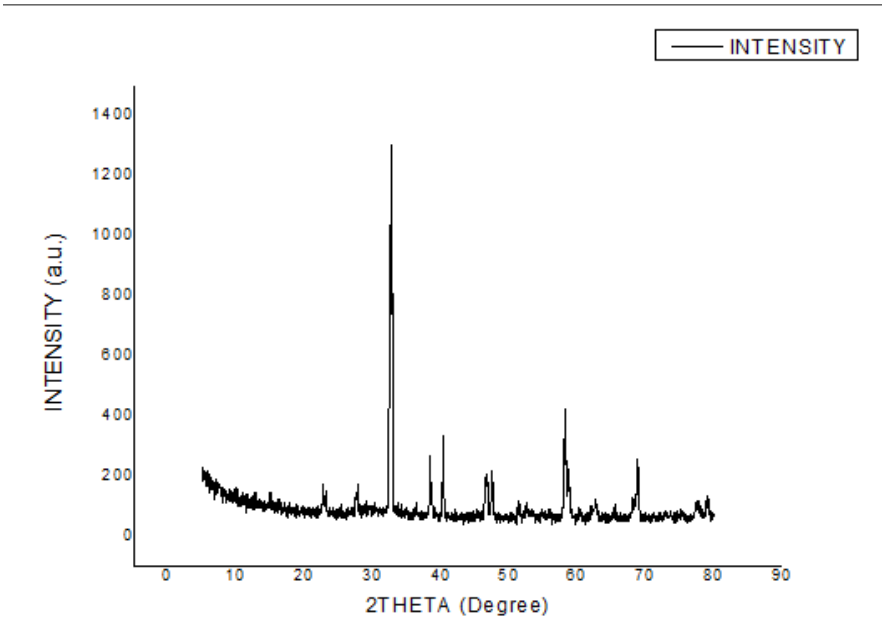

Figure 5.1. XRD pattern of YBCO target

The intensity each of pattern is showed their maximum 2θ values. Every sample was scanned between 2θ = 10^{o}-80^{o}. As mentioned in chapter 3, we used MgO substrate which is convenient to grow YBCO thin films. Figure 5.2 shows the XRD result of MgO substrate and its orientation.

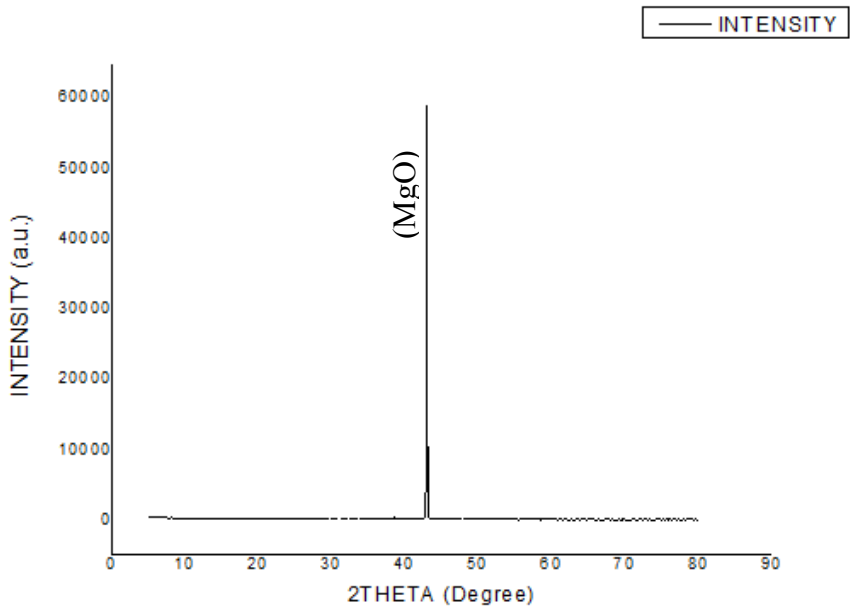

Figure 5.2. XRD pattern of MgO

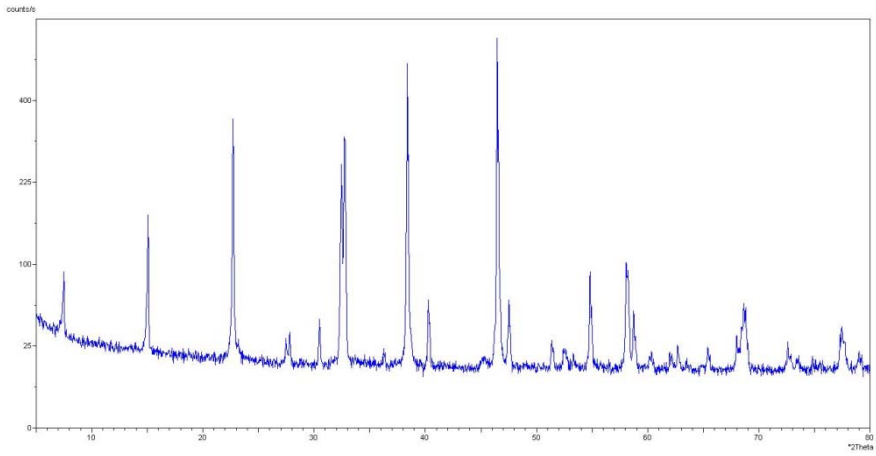

Figure 5.3. XRD pattern of YBCO-2

The x-ray diffraction pattern of YBCO thin film on MgO substrate showed only (00l) diffraction peak for YBCO layer. This indicates that the YBCO thin film is c-axis oriantated and epitaxial grown on MgO substrate.In the case of YBCO, the best films in terms of the superconducting properties were obtained when YBCO grown with the c-

axis oriented perpendicular to the surface. Therefore, only peaks related to the Miller indices (00l) are desired.

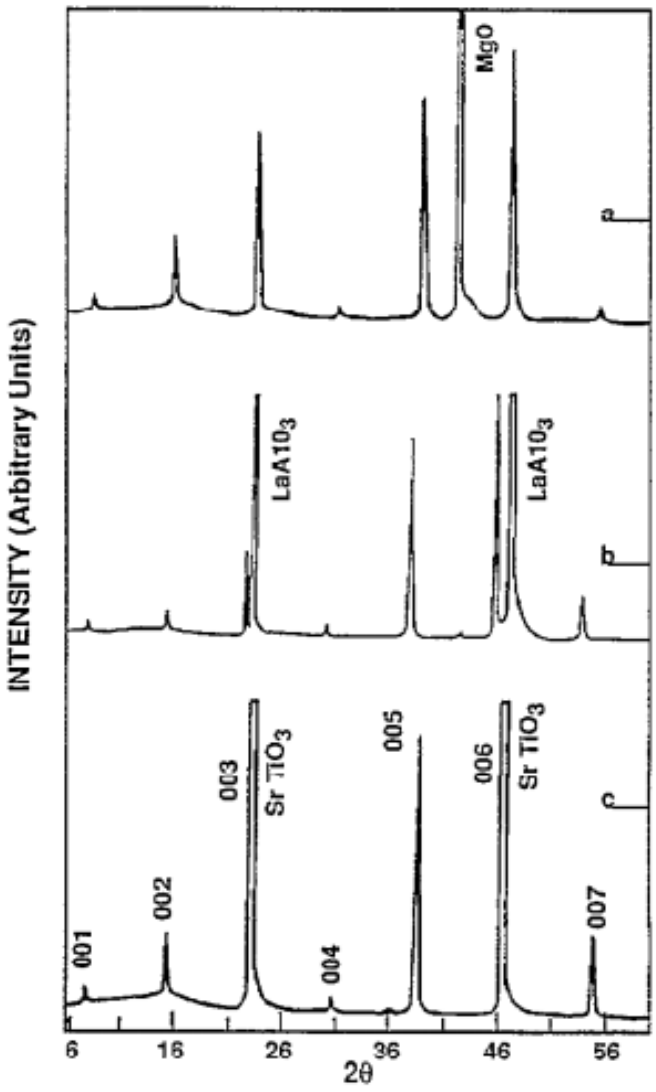

Figure 5.4. XRD patterns of MgO, $LaAlO_3$ and $SrTiO_3$
(Source: Singh, 1998)

5.2. SEM and EDX Results

In this study Scanning electron microscopy is PhilipsXL-30SFEG in Material Research Center at Izmır Instıtude of Technology, Turkey. It is equipped with a field emission electron gun owas used to examine the surface morphology. From the SEM images, there is a great difference and similarity in the surface morphology between our samples and the samples in literature (Proyer, 1996).

The proper target –substrate distance is very important for YBCO film grown by PLD system. If this distance is larger than 40mm, it is not easy for YBCO film to grown on MgO (100). Figure 5.3 shows the specific surface morphology of the film. It contains typical features for thick films as flower-like shapes made of particulates rich in $BaCuO_3$, Ba and Cu oxides (Branescu, 2007). Three different magnifications of the SEM pictures are displayed in the Figure 5.3. But if the target-substrate distance is too small, for example 20mm the (YBCO-1) as shown in Figure 5.4, there might be many droplets on the surface which is not fit layer. These droplets come from the drawback of PLD. During the ablation process of PLD, it is easy to eject micro-size particles from the target. If the target-substrate distance is not enough, those micro-sizeparticles will deposit on the substrate and form those droplets as Figure. In our experiment, the proper target-substrate distance is about 70mm which might result in a unique orientation and smooth surface under optimized condition. Figure 5.5. shows the smooth surface obtained at this proper distance.

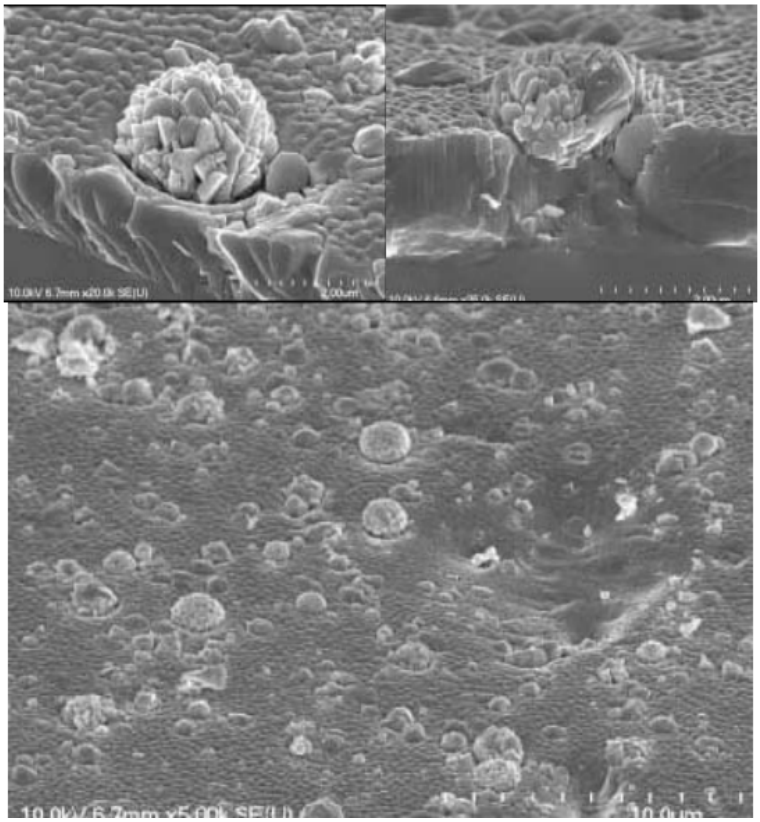

Figure 5.5. SEM micrographs of typical damaged surface of thin YBCO Film
(Source: Branescu, 2007)

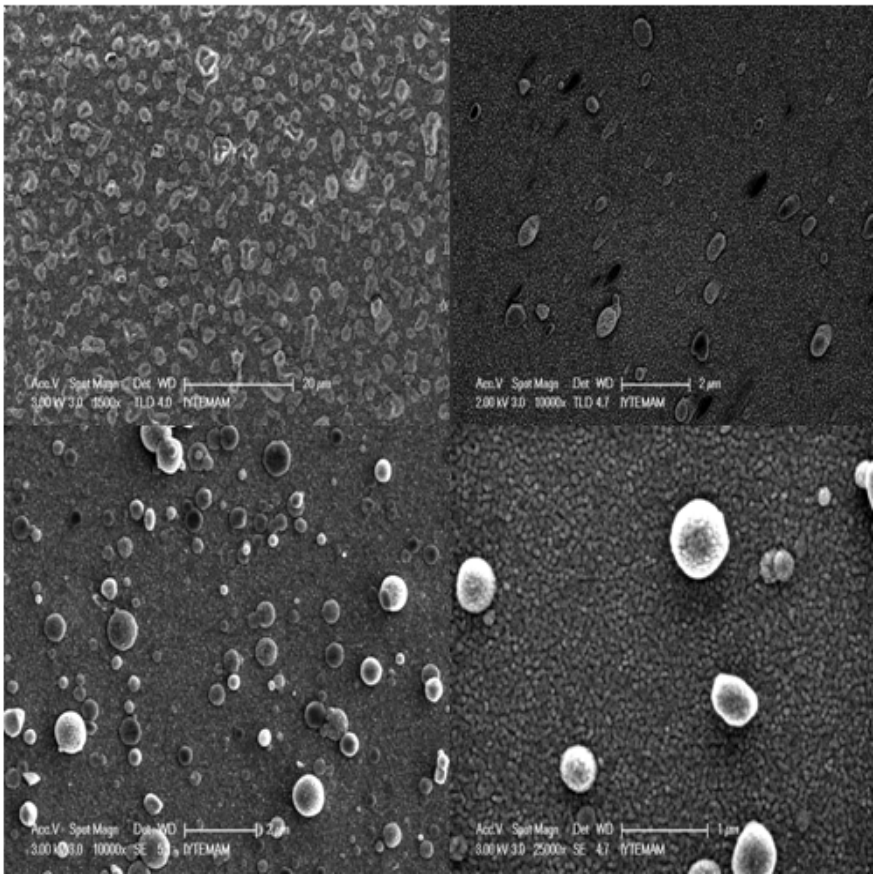

Figure 5.6. SEM images of YBCO films prepared with the target-substrate distance of 20mm this was deposited at 800 ^{o}C with oxygen pressure of 300mtorr

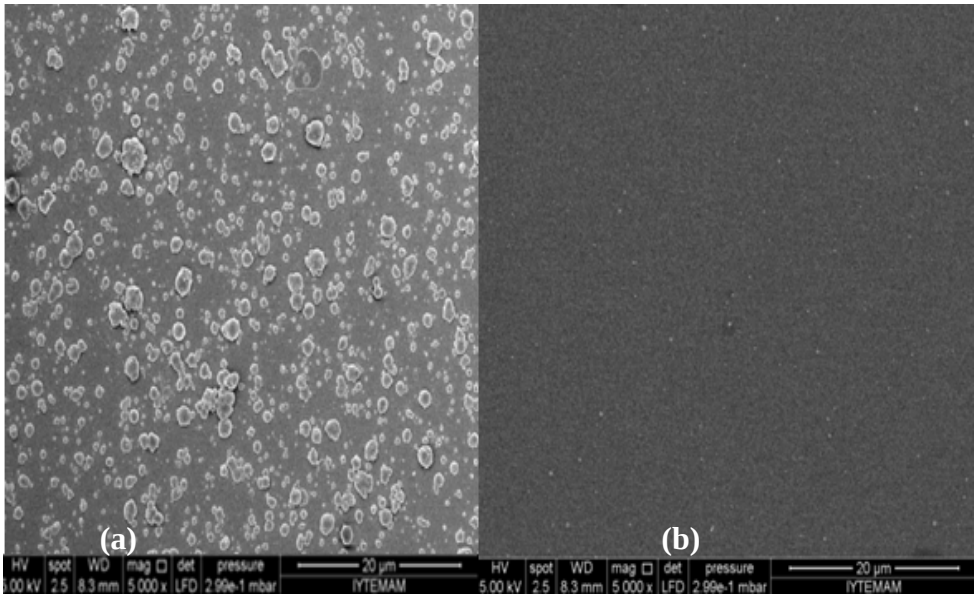

Figure 5. 7. (a) SEM images of YBCO films prepared with the target-substrate distance of 20 mm and (b) 75 mm. These films were deposited at 800^{o}C

Other method is Scanning Probe Microscopy (SPM), more commonly known as Atomic Force Microscopy (AFM), provides atomic or near-atomic-resolution surface topography, which is ideal for determining angstrom-scale surface roughness on a sample.The surfaces were imaged with a Nanoscope III (Digital Instruments, Santa Barbara, CA) atomic force microscope (AFM) apparatus in tapping mode. A Digital Instruments Multimode Nanoscope III scanning force microscope was used to obtain topographic data. Imaging was conducted in tapping mode, with 512x512 data acquisitions at a scan speed of 1.4 Hz at room temperature in air. Oxide-sharpened silicon nitride tips with integrated cantilevers with a nominal spring constant of 0.38 N/m were used. AFM images of the YBCO-4 sample growth on MgO surfaces were investigated after different pretreatments (Figure 5.8). Surface morphology on the MgO surfaces was determined using tapping mode AFM. The surface of the MgO substrate with some aggregated features was found on the clean film which indicated that the surface was not well clean Figure 5.8.A).The higher resolution of this image is given in the inset with scan area of 2x2 μm. The sample 5 surface with pretreatment of YBCO-4 showed more irregularities with new protuberances which were not observed in the clean membrane surface. This image indicated that the film start to have some particles arrangement or assembly after treatment with laser ablation as shown in higher resolution of image that given in figure B inset. However, the foulants after the physical pretreatments by YBCO-4 and YBCO-5 showed the balltype feature. The grain size was estimated from AFM line profile to be 100–300 nm. For more detailed information, the AFM roughness was measured.

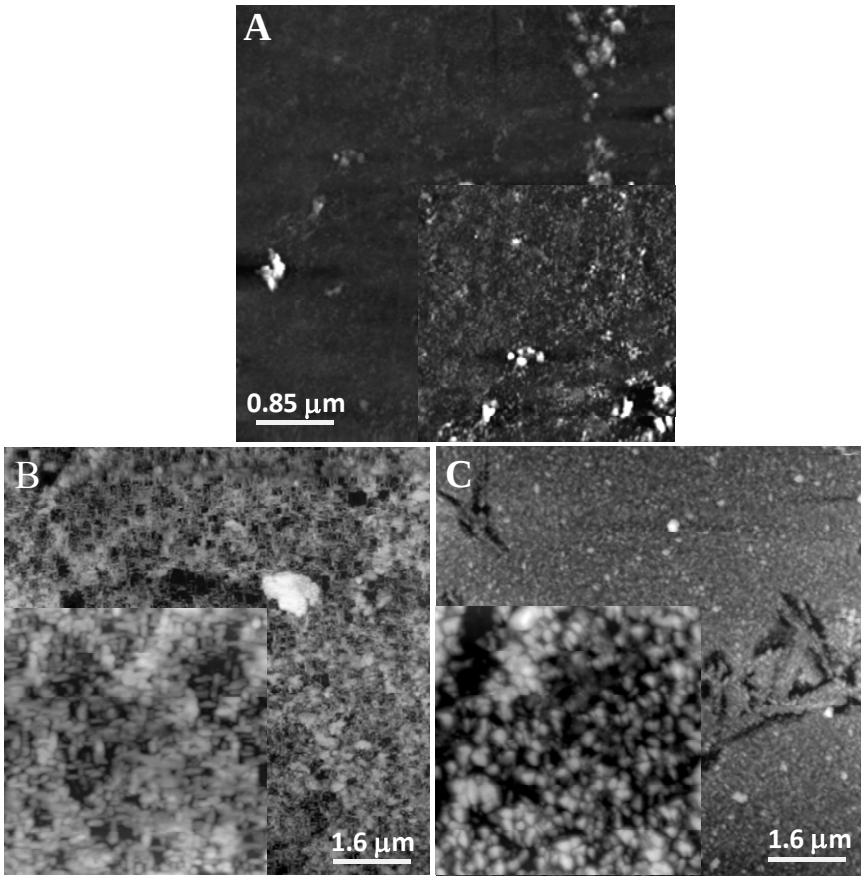

Figure 5.8. AFM surface roughness analysis of the YBCO-2 growth on on MgO

Energy Dispersive X-Ray (EDX) is a chemical microanalysis technique performed. In this technique, an electron beam of 10-20 keV strike the surface of a conducting sample that causes X-rays to be emitted from the point of incidence.the x-ray dedector measures the number of emitted x-rayswith respect to their energy. By collecting and analyzing the energy of these X-rays, the component elements of the specimen can be determined. EDX analysis results of the YBCO thin film are given Figure 5.8. From the EDX spectrum wwe identifies the elements Y, Ba, Cu, O and Mg present in the YBCO. From this analysis, there is no detectable impurity phase in the YBCO structure.

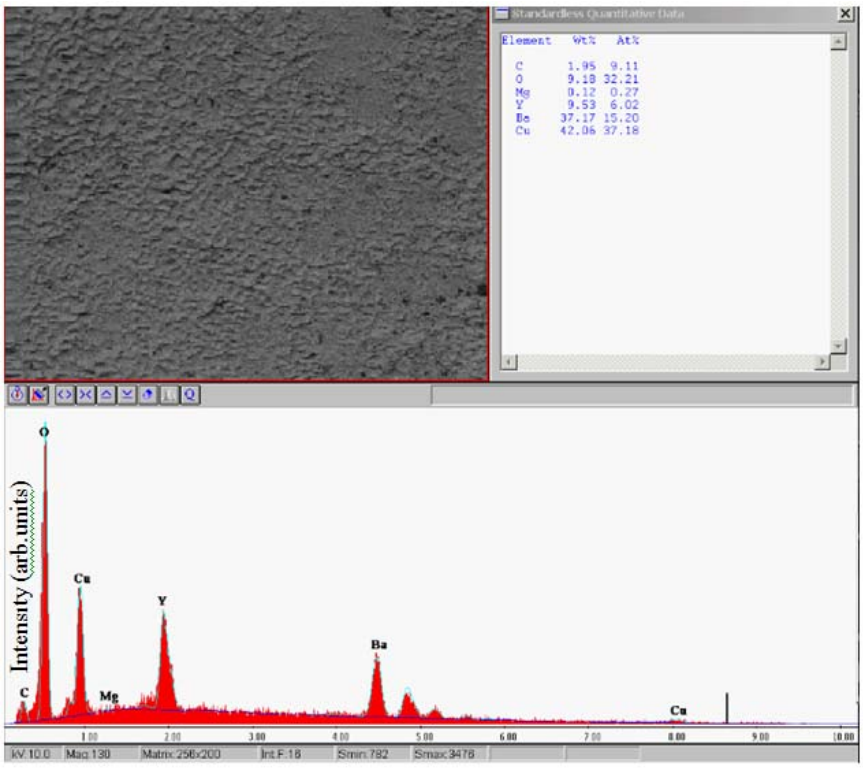

Figure 5.9. EDX analysis for the YBCO/MgO sample

5.3. Electrical Characterization Results

The superconductig onset transition temperature T_{onset}, and the critical temperature T_c, the temperature att which resistance vanishes completely, of the sample device were determined by resistance versus temperature (R-T) measurements at a constant current in four-point probe configuration. Contacts to the sample were provided using Ag wires, which were connected to the contact pads on the sample, using Ag paint. Apiezon or vacuum-grease was applied to the back of the substrate in order to provide good thermal contact between the sample and the cold head. The cold head is cooled down to 4K using closed cycle He-refrigerator. A Keithley 2400 voltage-current source and Nanovoltmeter was used to supply the bias current required to measure the voltage and the resistance changes with temperature. A Lakeshore 331 temperature controller kept of the temperature. All instruments were connected to a Computer which has labview program to facilitate data getting and experimental control. To calculate the parameters of temperature dependence of resistance measurements, dR/dT (Derivative of the Resistance) were taken. Mathematically, a

superconducting transition graph can be described as a step function. Hence, derivative of this graph give us a peak at the T_c value of the graph. From dR/dT $T_c^{zero}, T_c^{onset}, T_c^{mid}, \Delta T$ values can be calculated. Temperature which transition begins show superconducting properties, called onset the critical temperature. These parameters can describe the superconducting quality of the materials. At dR/dT , the maximum peak show the middle transition temperature point, T_c^{mid}. 10% of maximum peak values give the 90% and 10% values of the onset transition temperature. ΔT values can be determined by differences of these values. T_c of the sample was found to be around 80K and T_{onset} was found to be around 87K as shown in Figure 5.11. We realized that increasing annealing time for getting oxygen decreased the ΔT values some of the samples. While annealing time is 30 min at 500ºC for YBCO-2 sample, ΔT is bigger when compared literature.This changing in the ΔT can be dependent of the impurity of the films (Goo, 1999)

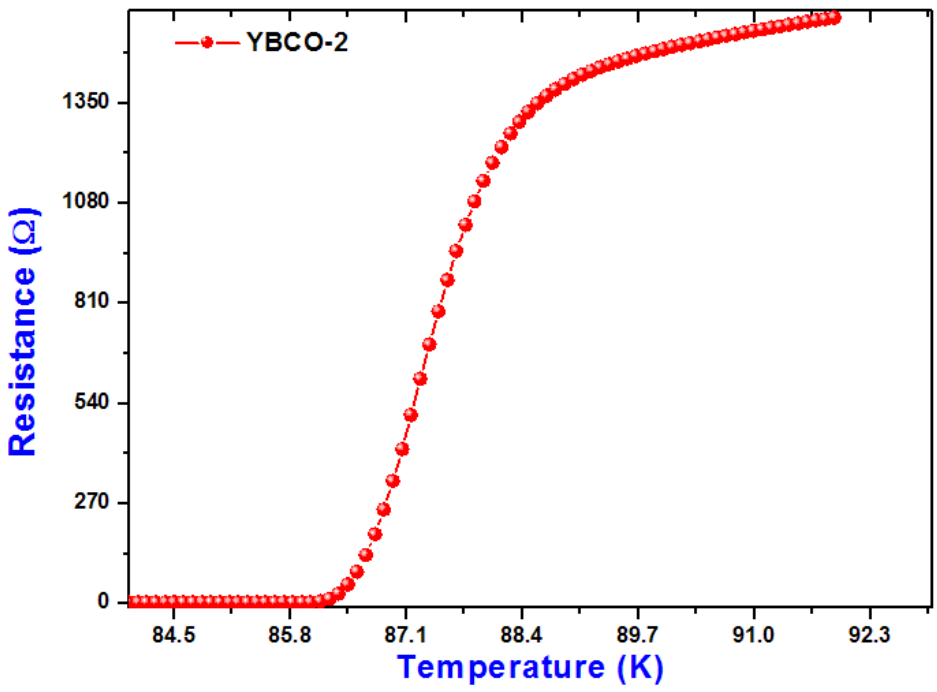

Figure 5.10. Resistance vs Temperature results of YBCO-2

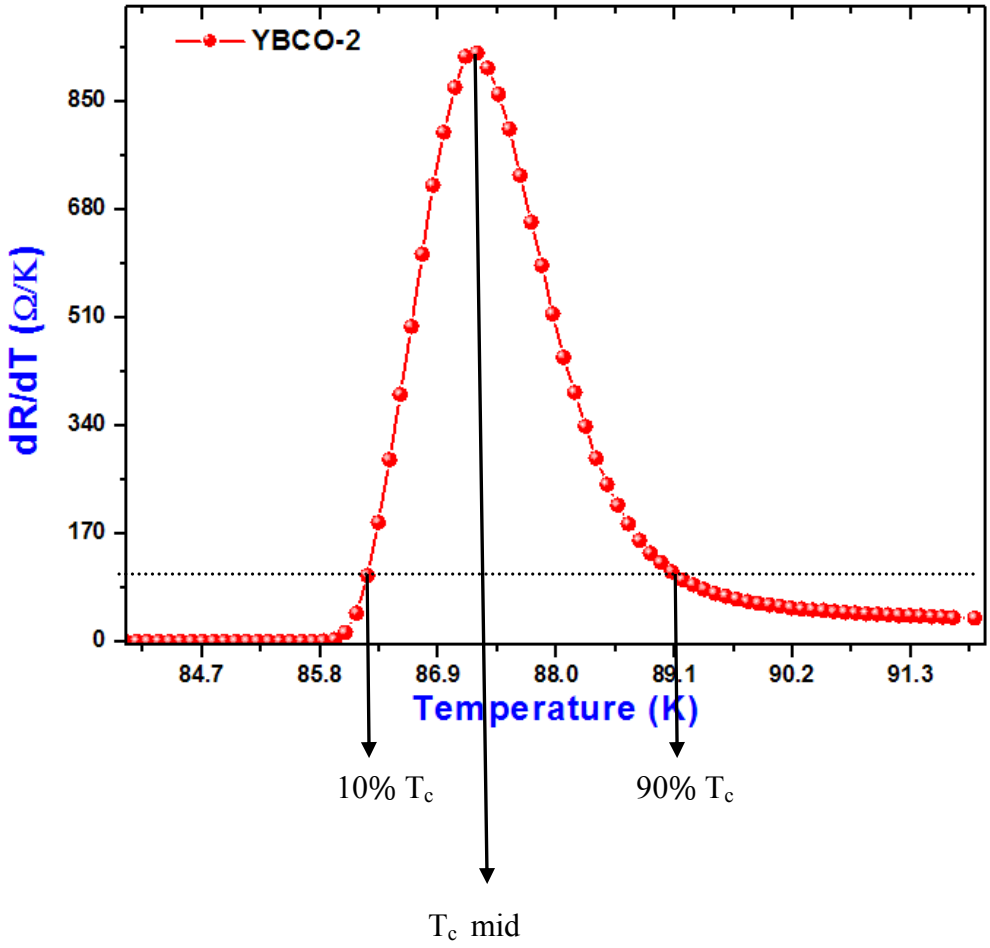

Figure 5.11. dR/dT –Temperature graph of YBCO-2

Temperature dependence resistance graphs for YBCO-2 film were shown in figure 5.10. The resistances values of YBCO film were normalized to 84 Kvalues of them. Figure 5.12 and figure 5.13 show the transition temperatures of the films deposited at different deposition parameters. We can observed the correlation between superconducting transition width, which is affected by the laser energy density and oxygen pressure and time. We obtained R-T graphs for changing oxygenation pressure and hold time. As shown in the figure 5.12 when oxygenation time increases critical temperature increases.

Table 5.1. Some deposition parameters of YBCO films grown on MgO

Sample	Laser Fluence (J/cm^2)	Rep. Rate (Hz)	Annealing (Torr)	Annealing Sub. Temp. (°C)	Hold Time During Annealing
#1	1.82	5hz	450-500 O_2	650	40′
#2	2.52	5hz	400 O_2	650	30′
#3	3.02	5hz	300 O_2	500	1 hour
#4	1.82	3hz	300 O_2	500	45′

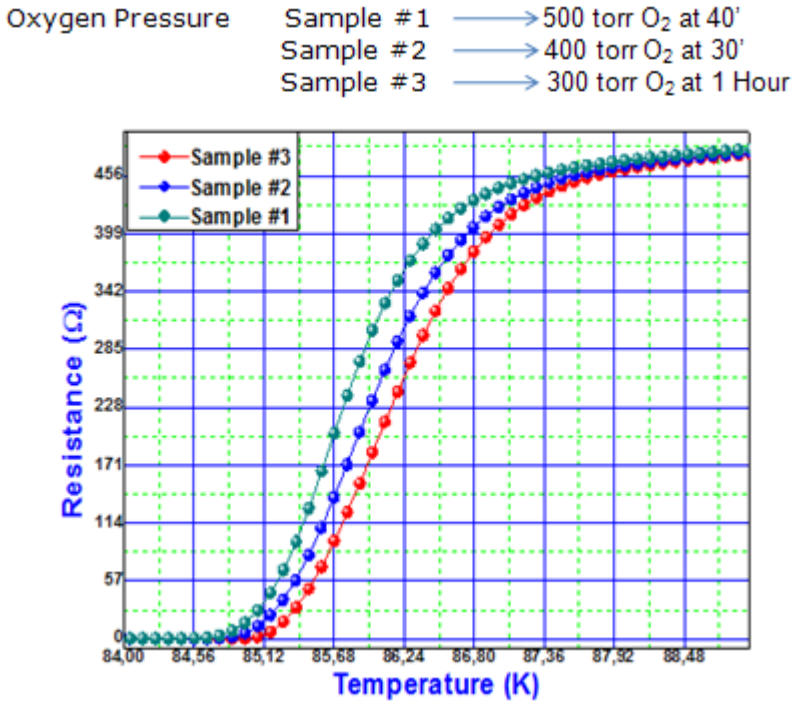

Figure 5.12. Dependence of oygenation pressure and time Resistance vs Temperature results of YBCO-2

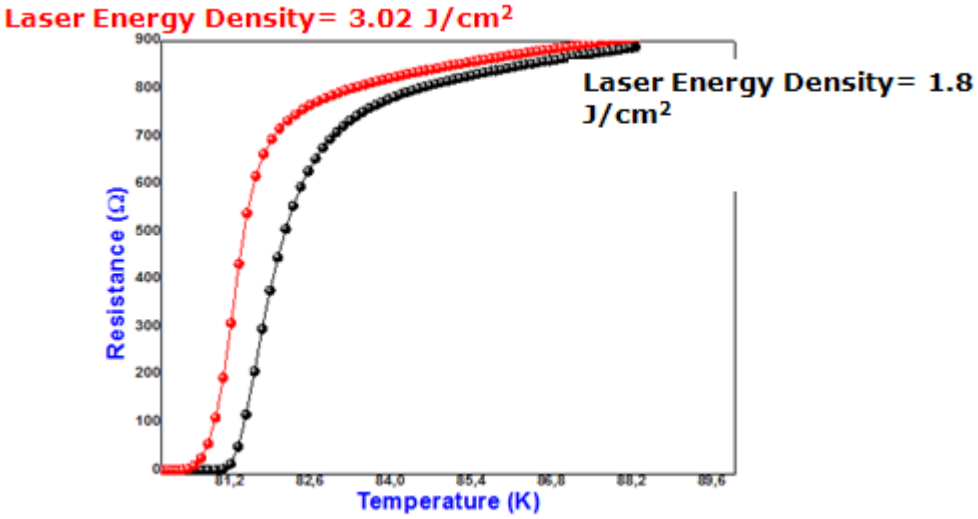

Figure 5.13. Dependence of laser energy density Resistance vs Temperature results of YBCO-2

Figure 5.13 shows depending on laser energy density. While the laser energy density was high, the transition temperature decreases because of particulations. Due to lots of particulation and impurities melted down on the surface of the substrate. It led to decrease the critical temperature. If the laser energy is small, we can obtain high quality superconducting films.

CHAPTER 6

CONCLUSIONS

Thin films of the high temperature superconductor $YBa_2Cu_3O_7$ offer great potential applications in the fabricaiton of superconducting electronic devices and large current carrying coated conductors, as well as having the potential to give insight into the fundamental mechanisms governing high temperature superconductivity. The results of a fundamental study is presented in this thesis on the fabrication of $YBa_2Cu_3O_7$ thin films using advanced thin film fabrication methods, including pulsed laser deposition system (PLD). PLD system uniquely offers controlled growth high quality YBCO thin films. The first thin film of a high temperature superconductor using the PLD tecnique was deposited in 1987 by Dijkkamp, while high temperature superconding film were epitaxially grown in 1989s.

We have produced, characterized and analyzed YBCO thin film. In our study, we tried to deposit YBCO thin films by using PLD system. Firstly, a YBCO composite target was produced using commerically available Y_2O_3, $BaCO_3$ and CuO which were mixed in ratio of Y: Ba: Cu = 1:2:3. YBCO thin films were grown on MgO substrates. The second step was carried out to perform YBCO thin film by PLD system *in-situ* annealing procedure. Various annealing temperature 600°C, 550°C, 500°C and various annealing times, 30 minutes and 60 minutes, were examined to increase the quality of YBCO films.

Our YBCO thin films were fabricated with two different surface qualities. The structural characterizations were performed by x-ray diffraction (XRD), scanning electron microscopy (SEM) and atomic force microscopy (AFM). All XRD data were taken 2θ region. The XRD results showed that some of them have main peak of YBCO in different quality. When compared the 60 min annealed sample at 550ºC become sharper than 500°C. At the 450 ºC, decreasing annealing time, we got bad results. The XRD results showed that our films are epitaxial and c-oriented when the deposition temperature is between 750 ºC and 800ºC. The other structural characterization is The SEM which gives us information about surface morphology. According to some SEM and AFM images, droplets were seen on the surface. The major technical obstacle of

particulates emission was big problem. Owing to particulates, our films are insulator. From AFM images, we saw that some particulates were melt on the surface. Encountered initially with PLD has been solved that we changed distance between target and substrate until the surface was smooth.

For YBCO thin films grown on MgO, it is found that the deposition conditions are crucial for making high quality YBCO thin films using the PLD technique, since the superconductivity of YBCO compound is very sensitive to the oxygen content. It has been found that a wide range of deposition conditions resulted in a good c-alignment, which was obtained. However, the values of T_c and the transition widths are highly dependent on several important conditions, such as the laser pulse energy (E), oxygen preessure, substrate temperature, and distance between target and substrate. In this work, we found that substrate temperature should be around 550°C. Laser energy density should be small, distance between substrate and target about 45mm, and oxygen pressure 300-400 mtorr for making good quality films. At low temperature and pressure we did not found any transition.Changing this parameters we have obtained YBCO superconducting films. After electrical characterization,resistance versus temperature (R-T), we found transition temperature around 85K. It has different while compared with literature about YBCO thin film prepared PLD system.

As a conclusion, we achieved to product a YBCO target for PLD system. To deposit superconducting YBCO thin film, a high vacuum pulsed laser deposition system was used. To enhance the superconducting properties of the films and to increase the crystal quality of the prepared films an in-situ annealing process was performed. Annealing process and deposition parameters develops the structure and electrical properties of the films. When applied available depostion parameters such as substrate temperature, laser energy, oxygen pressure and oxygenation time, we can obtain good quality films.

REFERENCES

Abrikosov, A. 1957. On the magnetic properties of superconductors of second. Group. Sov. Phys. FETP 5:1174-1182.

Afonso, C.N., J. Gonzalo, R. Serna, J. Solis. 2007. Pulsed Laser Deposition For Functional Optical Films. Optical Science 129:315-319.

Afonso, C.N., R. Serna, F. Catalina, D. Bermejo. 1990. Good-quality Ge films grown by excimer laser deposition. Applied Surface Science Vol 46: 249-253.

Ba¨r, S. 2004. Cystalline Rare-Earth-doped sesquioxide PLD-Films on alpha-aluminia. Göttingen.

Bardeen, J., L.N. Cooper, J.R. Schrieffer. 1957. Microscopic theory of superconductivity. Phys. Rev 106:162-164.

Bednorz, J.G., K.A. Müller. 1986. Perovskite-type oxides-The new approach to high-T_c.

Bernhard, C., J.L. Tallon. 1996. Low-temperature critical current of $YBa_2Cu_3O_{7-x}$ thin films as a function of hole content and oxygen deficiency. Phys Rev 51:10201.

Blank, D.H.A., R.P.J. IJsselstteijn, P.G. Out, H.J.H. Kuiper, J.Floksura, H. Rogalla. Mater. Sci. Eng. B13:67.

Branescu, M., M. Ward, I. Huh, J. Matsushita, Y. Zeltzer. 2007. Scanning electron microscopy and resistive transiton of in-situ grown YBCO films by pulsed laser deposition. G 1088: 1742-6596.

Chrisey, D.B., G.K.Hubler. 1994. Pulsed Laser Deposition of Thin Films. Willey.

Doughty, C., A.T. Findikoglu, T. Venkatesan. 1995. Steady state pulsed laser deposition target scanning for improved plume stability and reduced particle density. Journal of Applied Physics Letter 66:1276.

Ellmer, K., A.Klein, B.Rech. 2008. Transparent Conductive Zinc Oxide. Springer.

Goo, D., D. Youm, J. Yoo, K. Ahn, J. Yoon. 1999. Fabrication of growth of textured YBCO thin film on very thin metallic substrate. Physica C: 282-287.

Guo, R., A.S., Bhalia, L.E. Cross, R. Roy, J. Mater. 1994. Applicaiton of high –temperature superconductors in microwave integrated circuits. Res. 9:1644.

Hollmann, E.K., O.G. Vendik, A.G. Zaitsev, B.T. Melekh. 1994. Substrates for high-Tc superconductor microwave integrated circuits. Supercond. Sci. 7: 609.

Houdy, P.H., J.A. Sirat, J.B. Theetin, J.P. Landesman, H. Buadry, M. Monneeraye, C. Schiller, J.N. Patillon. 1987. Pulsed laser deposition and characterization of high-Tc $YBa_2Cu_3O_{7-x}$ superconducting thin films. AIP Conf 165:122.

Jaakkola A. 2003. Thesis of Laser Ablation and Thin-Film Deposition.

James D. Doss. 1989. Engineer's Guide to High Temperature Superconductivity. Wiley, New York.

Jorgensen, J.D., B.W. Veal, A.P. Paulikas, L.J. Nowicki, G.W. Crabtree, H. Claus and W.K. Kwok. 1990. Structural properties of oxygen-deficient YBa2Cu3O7-δ . Phys. Rev. B 41:1863.

Krebs, H.U., M.Weisheit, J.Faupel, E.Süske, T.Scharf, C.Fuhse, M.Störmer, K.Sturm, M.Seibt, H.Kijewski, D.Nelke, E.Panchenko, M.Buback. 2003. Pulsed Laser Deposition (PLD)-a Versatile Thin Film Technique. Advance in Solid State Physics Vol 43: 101-107.

Larbalestier, D., A. Gurevich, D.M. Feldmann, A. Polyanskii. 2001. High Tc superconducting materials for electric power applications. Nature 414:368-377.

Lenk, A., B. Schultrich, T. Witke, H.J. Weiß. 1997. Energy and Particle Fluxes in PLD Processes. Applied Surface Science 109-110:419-423.

Lunney, J.G., R.Jordan. 1998. Pulsed Laser Ablation of Metals. Applied Surface Science 127-129: 941-946.

Maeda H, Y. Tanaka, M. Fukutomi, T. Asano. 1988. A new high-r.oxide superconductor without a rare element. Phys 27: 209-210.

Mogro, A., L.G. Turner, E.L. Hall.1989. LaAlO3 single crystal substrate for epitaxial superconducting thin films. Journal of Applied Physics 65:1451.

Naito, M., R.H. Hammond, B. Oh, M.R. Hahn, J.W.P. Hsu, P. Rossenthal, A.F. Marshall, M.R. Beasley, T.H. Geballe, A. Kapitnlink, J. Mater. 1987. Superconductivity behaviour in screen-printed $YBa_2Cu_3O_7$ films. Res 2:713.

Nakayama, T., M. Okiwaga, N. Itoh. 1984. Laser-induced sputtering of oxides and compound semiconductors. Nucl. Instrum. Meth B 1:301.

Niu, C., C.M. Lieber. 2006. Thin Film Synthesis of Solids, Harvard University, Cambridge, MA, USA.

Ohmukai, M., T. Fujita, T. Ohno. 2001. The Temperature Dependence of Critical Current in $YBa_2Cu_3O_{7-\delta}$ thin films deposited on MgO by an eclipse PLD. Brazilian Journal of Physics Vol 31:3.

Onnes, H.K. 1911. The disappearance of the resistivity of mercury. Common Leiden.

Pechen, E.V., A.V. Varlashkin, S.I.Krasnosvobodtsev, B.Brunner, and K.F.Renk. 1995. Laser Deposition of smooth High-Tc superconducting Films Using Velocity Filtration of plasma particles. Journal Applied Phyics Letter 66:2292.

Phillips, J.M. 1996. Epitaxial $YBa_2Cu_3O_{7-\delta}$—Ag thin films (Jc = 6 × 106 A/cm2) on epitaxial films of Ba2LaNbO6, a new perovskite substrate, by pulsed laser ablation. Journal of Applied Physics 79: 1829.

Pinto,R., S.P. Pai, L.C. Gupta, R. Vijayaraghavan, A.G. Choure, V.S. Shirodkar. 1990. Pulsed laser deposition and characterization of high-Tc $YBa_2Cu_3O_7$ − xsuperconducting thin films. Pysica C: 131-171.

Poole, C. 1995. Superconductivity. Elsevier P: 545-570.

Prieto, U., J. Schubert, H. Soltner, K. Urban, Ch. Buchal. 1989. Epitaxial multilayers of $YBa_2Cu_3O_{7-\delta}$ and $PrBa_2Cu_3O_7$ as a possible basis for superconducting electronic devices. Solid State Commun. 71:569.

Proyer, S., Stangl, E., Borz, M., Hellebrand, B., Bäuerle. 1996. Particulates on pulsed laser deposited Y-BA-Cu-O films 257: 1-15.

Schou, J. 2009. Physical Aspects of Pulsed Laser Deposition Technique: The Stoichiometric Transfer of Material From Target to Film. Applied Surface Science 255:5191-5198.

Singh, R.K., L. Ganapati, P. Tiwar, J. Narayan. 1989. Pulsed laser deposition and characterization of high-Tc $YBa_2Cu_3O_{7-x}$ superconducting thin films. Journal of Applied Physics Letter 55:2351.

Singh, R.K. 1998. Pulsed laser deposition and characterization of high-Tc $YBa_2Cu_3O_{7-x}$ films. Elseviever 113: 185.

Somekh, R.E., M.G. Blamire, Z.H. Barber, K. Buttler, J.H. James,G.W. Morris, E.J. Tomlinson, A.P. Schwarzenberger, W.M. Stobb, J.E. Evetts. 1987. Pulsed laser deposition and characterization of high-Tc $YBa_2Cu_3O_{7-x}$superconducting thin films.

Tallon, J.L., C. Bernhard, H. Shaked, R. L. Hitterman, and J. D. Jorgensen. 1995. Pulsed laser deposition and characterization of high-Tc $YBa_2Cu_3O_{7-x}$ superconducting thin films. Phys Rev 51: 1291.

Venkatesan, T., S.M.Green. 1996. Pulsed Laser Deposition: Thin Films in a Flash. American Institute of Physics.

Willmott, P.R., J.R. Huber. 2000. Pulsed Laser Vaporization and Deposition. Reviews of Modern Physics Vol 72:1.

Wu, M.K., J.R. Ashburn, C. J. Torng, P.H. Hor, R.L. Meng, L. Gao, Z.J. Huang, Y.Q. Wang, C.W. Chu. 1987. Superconductivity at 93 K in a new mixed-phase Y-Ba-Cu-O compound system at ambient pressure. Phys 58: 908-910.

Yamane, H., H. Kurosawa, T. Hirai, K. Watanabe, H. Iwasaki, N. Kobayashi, Y. Muto. 1989. Low-temperature formation of $YBa_2Cu_3O_{7-\delta}$ superconducting films by thermal CVD and their Jc in high magnetic fields. Supercond. Sci. Technol. 2:115.

Z Liu, Z., G.J., Bowden. 1991. and G J Bowden. 1991. Viscous flux flow in the Bean model of type II superconductors. Supercond. Sci. Technol. 4: 122-127.

Zheng, P., Q.Y. Ying, S.Witanachchi, Z.Q. Huang, D.T. Shaw, H.S. Kwok. 1989. The Role of the Oxygen Atomic Beam in Low Temperature Growth of Superconducting Films by Laser Deposition. Journal of Applied Physics Letter 54:954.